

Extracellular vesicles from human-induced pluripotent stem cell-derived neural stem cells alleviate proinflammatory cascades within disease-associated microglia in Alzheimer's disease

Leelavathi N. Madhu¹ | Maheedhar Kodali¹ | Raghavendra Upadhya¹ | Shama Rao¹ |
Yogish Somayaji¹ | Sahithi Attaluri¹ | Bing Shuai¹ | Maha Kirmani¹ | Shreyan Gupta² |
Nathaniel Maness¹ | Xiaolan Rao¹ | James J. Cai² | Ashok K. Shetty¹ 

¹Institute for Regenerative Medicine, Department of Cell Biology and Genetics, College of Medicine, Texas A&M University Health Science Center, College Station, Texas, USA

²Department of Veterinary Integrative Biosciences, Texas A&M College of Veterinary Medicine, College Station, Texas, USA

Correspondence

Ashok K. Shetty, University Distinguished Professor and Associate Director, Institute for Regenerative Medicine, Department of Cell Biology and Genetics, College of Medicine, Texas A&M University Health Science Center, 1114 TAMU, 206 Olsen Boulevard, College Station, TX 77843, USA.
Email: ash.shetty@tamu.edu

Funding information

National Institute on Aging, Grant/Award Numbers: IRF1AG074256-01, R01AG075440-01

Abstract

As current treatments for Alzheimer's disease (AD) lack disease-modifying interventions, novel therapies capable of restraining AD progression and maintaining better brain function have great significance. Anti-inflammatory extracellular vesicles (EVs) derived from human induced pluripotent stem cell (hiPSC)-derived neural stem cells (NSCs) hold promise as a disease-modifying biologic for AD. This study directly addressed this issue by examining the effects of intranasal (IN) administrations of hiPSC-NSC-EVs in 3-month-old 5xFAD mice. IN administered hiPSC-NSC-EVs incorporated into microglia, including plaque-associated microglia, and encountered astrocyte soma and processes in the brain. Single-cell RNA sequencing revealed transcriptomic changes indicative of diminished activation of microglia and astrocytes. Multiple genes linked to disease-associated microglia, NOD-, LRR-, and pyrin domain-containing protein 3 (NLRP3)-inflammasome and interferon-1 (IFN-1) signalling displayed reduced expression in microglia. Adding hiPSC-NSC-EVs to cultured human microglia challenged with amyloid-beta oligomers resulted in similar effects. Astrocytes also displayed reduced expression of genes linked to IFN-1 and interleukin-6 signalling. Furthermore, the modulatory effects of hiPSC-NSC-EVs on microglia in the hippocampus persisted 2 months post-EV treatment without impacting their phagocytosis function. Such effects were evidenced by reductions in microglial clusters and inflammasome complexes, concentrations of mediators, and end products of NLRP3 inflammasome activation, the expression of genes and/or proteins involved in the activation of p38/mitogen-activated protein kinase and IFN-1 signalling, and unaltered phagocytosis function. The extent of astrocyte hypertrophy, amyloid-beta plaques, and p-tau were also reduced in the hippocampus. Such modulatory effects of hiPSC-NSC-EVs also led to better cognitive and mood function. Thus, early hiPSC-NSC-EV intervention in AD can maintain better brain function by reducing adverse neuroinflammatory signalling cascades, amyloid-beta plaque load, and p-tau. These results reflect the first demonstration of the efficacy of hiPSC-NSC-EVs to restrain neuroinflammatory signalling cascades in an AD model by inducing transcriptomic changes in activated microglia and reactive astrocytes.

This is an open access article under the terms of the [Creative Commons Attribution-NonCommercial-NoDerivs License](https://creativecommons.org/licenses/by-nc-nd/4.0/), which permits use and distribution in any medium, provided the original work is properly cited, the use is non-commercial and no modifications or adaptations are made.

© 2024 The Author(s). *Journal of Extracellular Vesicles* published by Wiley Periodicals LLC on behalf of International Society for Extracellular Vesicles.

KEYWORDS

Anti-inflammatory effects, disease-associated microglia, extracellular vesicles, human induced pluripotent stem cell-derived neural stem cells, inflammasomes, interferon 1 signalling, mitogen-activated protein kinase signalling

1 | INTRODUCTION

The pathological changes associated with cognitive and mood impairments in Alzheimer's disease (AD) include lasting neuroinflammation, extracellular deposition of amyloid-beta 42 ($A\beta_{42}$) plaques, intraneuronal neurofibrillary tangles, synapse loss, hyperphosphorylated tau (p-tau), and neurodegeneration (Duyckaerts et al., 2009; Long & Holtzman, 2019; Selkoe, 1989; van der Kant et al., 2020). Deposition of $A\beta$ plaques likely contributes to the progression of neuroinflammation, the loss of synapses, p-tau accumulation, and neurodegeneration (Long & Holtzman, 2019). Current therapeutic strategies for AD are not efficacious in slowing its progression (Yiannopoulou et al., 2019). Therefore, novel therapies proficient in restraining the progression of multiple pathological changes, including neuroinflammatory signalling cascades, and maintaining better cognitive and mood function for extended periods after the initial AD diagnosis have great significance (Long & Holtzman, 2019).

Transplantation of neural stem/progenitor cells (NSCs), derived from various sources, including the human induced pluripotent stem cells (hiPSCs) has improved function in several brain disease models (Eckert et al., 2015; Hattiangady & Shetty, 2012; Lu et al., 2021; Shetty & Upadhyia, 2016; Temple, 2023). However, multiple safety issues have hampered the clinical translation of hiPSC-derived NSC grafts (Attwood & Edel, 2019; Martin, 2017). Moreover, unlike other brain diseases, NSC grafting for AD is challenging as it involves pathological alterations in multiple brain regions (Abdi et al., 2022; Temple, 2023; Upadhyia et al., 2019). Besides, the functional recovery after NSC grafting has been mainly attributed to the secretome of the NSC graft-derived cells (Eckert et al., 2015; Willis et al., 2020). Also, the vital component of the NSC secretome has been identified as extracellular vesicles (EVs), as they facilitate the transfer of genetic information and proteins from NSCs into host cells (Willis et al., 2020). EVs, carrying a cargo of miRNAs and proteins from parental cells, can modify the function of recipient cells by transferring components (Cossetti et al., 2014; Iraci et al., 2017; Morton et al., 2018). Therefore, NSC-derived EVs, likely retaining most of the therapeutic effects of NSCs, can promote a cell-free therapy for AD (Ayyubova et al., 2023; Hering & Shetty, 2023; Upadhyia et al., 2020). Indeed, EVs derived from hiPSC-NSCs (hiPSC-NSC-EVs) have robust therapeutic properties because of anti-inflammatory miRNAs and proteins carried by them (Upadhyia et al., 2020, 2022). Additionally, hiPSC-NSC-EVs are a much safer alternative to hiPSC-NSCs, as they do not replicate, and can readily cross the blood-brain barrier. EVs are also amenable for repeated, non-invasive intranasal (IN) dispensation as an allogeneic off-the-shelf product for treating neurodegenerative diseases because EVs can be stored frozen and used immediately after thawing without losing their biological activity. Furthermore, EVs quickly permeate the entire brain after an IN administration, including in an AD model (Attaluri et al., 2023; Kodali et al., 2023a, 2023b; Long et al., 2017).

Therefore, using 3-month-old 5x familial AD (5xFAD) mice, we investigated whether IN administrations of hiPSC-NSC-EVs in the early stage of AD would moderate the activation of microglia and astrocytes, the associated neuroinflammatory signalling cascades, $A\beta$ plaques, and p-tau, leading to better cognitive and mood function. These EVs, purified from hiPSC-NSC culture media using anion-exchange and size-exclusion chromatographic methods, naturally carry a cargo of anti-inflammatory miRNAs and proteins (Upadhyia et al., 2020, 2022). Single-cell RNA-sequencing (scRNA-seq) revealed the proficiency of hiPSC-NSC-EVs to modulate multiple genes linked to activation of disease-associated microglia (DAM), NOD-, LRR-, and pyrin domain-containing protein 3 (NLRP3)-inflammasomes, and interferon-1 (IFN-1) signalling in microglia, and IFN-1 and interleukin-6 (IL-6) signalling in astrocytes. The modulatory effects of hiPSC-NSC-EVs on microglia persisted even 2 months post-treatment in the hippocampus without impacting their phagocytosis function, perceptible from reduced concentrations of proteins and/or genes causing the activation of NLRP3 inflammasomes and p38/mitogen-activated protein kinase (p38/MAPK) signalling and unaltered phagocytosis function. Additionally, proteins involved in the cyclic GMP-AMP synthase and stimulator of interferon genes (cGAS-STING) pathway that activate IFN-1 signalling genes were also reduced in the hippocampus. These changes led to reductions in astrocyte hypertrophy, $A\beta$, and p-tau, and better cognitive and mood function. These results reflect the first demonstration of the efficacy of hiPSC-NSC-EVs to restrain neuroinflammatory signalling cascades in an AD model by inducing beneficial transcriptomic changes in activated microglia and reactive astrocytes.

2 | METHODS

2.1 | Culturing of hiPSC-derived NSCs, purification and characterization of hiPSC-NSC-EVs

Protocols for generating NSCs from hiPSCs (IMR90-4; Wisconsin International Stem Cell Bank, Madison, WI, USA), culturing of hiPSC-NSCs, isolating hiPSC-NSC-EVs using anion-exchange and size-exclusion chromatographic methods, characterizing EVs

for various markers and ultrastructure are detailed in our previous studies (Upadhyaya et al., 2020, 2022) and the [supplementary file](#).

2.2 | Animals and study design

Both transgenic 5xFAD mice and their background (wild type) strain (B6SJL/F1/J) were purchased from Jackson Labs (Cat No: 34840-JAX and 100012-JAX, Bar Harbor, Maine, USA) and maintained in our laboratory on B6/SJL genetic background by crossing 5xFAD transgenic male mice with B6SJL/F1/J female mice. The animal care and use committee of Texas A&M University approved all studies conducted in this investigation. Two cohorts of 3-month-old 5xFAD mice were randomly assigned to vehicle (Veh) or hiPSC-NSC-EVs groups (AD-Veh group, $n = 26$, 14 males and 12 females; AD-EVs group, $n = 27$, 13 males and 14 females). A group of age-matched naïve control animals ($n = 24$, 12 males and 12 females) served as the naïve group for neurobehavioral, immunohistochemical, and molecular studies. A separate set of animals ($n = 2$ /group, males) were employed for the initial scRNA-seq study. Furthermore, previously harvested brain tissues from four AD mice (males) that received IN administrations of hiPSC-NSC-EVs were used to assess the interaction of IN-administered PKH26-labeled hiPSC-NSC-EVs into microglia including plaque-associated microglia (PAM,) and astrocytes in the hippocampus (Attaluri et al., 2023). Additional AD mice receiving Veh or EVs ($n = 5$ /group) were employed for evaluating phagocytosis activity of microglia in vivo using methoxy-X04 (m-X04) injections.

2.3 | Administration of hiPSC-NSC-EVs

Animals in AD-EVs and AD-Veh groups received IN administration of hiPSC-NSC-EVs or vehicle (sterile phosphate buffered saline, PBS). In each animal, following mild anaesthesia, both nostrils were first treated with 10 μ L of hyaluronidase (100 U; H3506; Sigma-Aldrich, St. Louis, MO, USA) in PBS to enhance the permeability of the nasal mucous membrane. Thirty minutes later, each mouse was gently held with the ventral side up, and the head was facing downward for the IN administration of EVs or PBS. EVs were suspended in PBS at a concentration of 30×10^9 /100 μ L and dispensed into both nostrils in 5- μ L spurts separated by 5 min. The animals received two doses of 30×10^9 EVs or Veh with a 1-week interval between doses. Since 5xFAD mice is a rapidly progressing model of AD associated with severe neuroinflammation, we chose to test a relatively higher dose of hiPSC-NSC-EVs (i.e., 30×10^9 EVs, once weekly for 2 weeks) compared to lower doses of hiPSC-NSC-EVs (3.3×10^9 EVs, once every other day for 6 days, total, $\sim 10 \times 10^9$ EVs) employed in our previous study in a mouse model of peripheral inflammation-induced cognitive dysfunction (Ayyubova et al., 2023). The 5xFAD mice employed for the scRNA-seq study and phagocytosis activity of microglia in vivo also received two doses of 30×10^9 EVs or Veh, as described above.

2.4 | Isolation of live microglia and astrocytes from 5xFAD and naïve control mice and scRNA-seq studies

The 5xFAD mice were euthanized, and fresh brains were harvested 72 h after the last dose of EV/Veh administration and processed immediately for the isolation of live microglia and astrocytes. The microglia and astrocytes were also isolated from the age-matched naïve control mice. The brain tissues from two animals were pooled in every group and processed for live single-cell suspension preparation using gentleMACS Tissue Dissociator (Miltenyi Biotec, Gaithersburg, MD, USA). The cell suspensions were incubated with microbeads coated with specific primary antibodies, that is, CD11b for microglia and astrocyte cell surface antigen-1 (ASCA1) for astrocytes (Miltenyi Biotec) and subjected to magnetic cell isolation through MACS Separators to isolate microglia and astrocytes. Following live cell analysis and quality control measures, live microglia and astrocytes were subjected to the scRNA-seq targeting $\sim 10,000$ cells per sample at the Texas A&M Institute for Genome Sciences and Society facility. Individually barcoded libraries were pooled and sequenced on a NextSeq mid-output paired-end sequencing run at 2×75 using NextSeq 500/550 Mid-Output v2.5 kit (Illumina, San Diego, CA, USA) according to the manufacturer's instructions. The reads of scRNA libraries were aligned to the human GRCh38.p13 reference genome using Cell Ranger (version 7.0), and the resulting expression matrices were analysed using scGEAToolbox (Cai, 2020).

2.5 | Analysis of hiPSC-NSC-EVs effects on cultured hiPSC-derived microglia exposed to A β 42 oligomers

A method described in a published protocol was employed to generate microglia from hiPSCs (Guttikonda et al., 2021). These microglia are referred to as iMicroglia from here onwards, and additional details on iMicroglia are available in the [supplementary file](#). Three sets of mature iMicroglia were cultured on a Petri plate ($n = 8$), of which two sets were exposed to A β 42 oligomers

at a concentration of 1 μM . The dose of $\text{A}\beta_{42}$ oligomers chosen for this assay was based on a published study demonstrating that exposure of primary microglia or BV2 microglia to 5 μM or higher doses of $\text{A}\beta_{42}$ oligomers induces cell death, but 0.2–1.0 μM doses do not induce microglial cell death (Pan et al., 2011). Four hours after adding $\text{A}\beta_{42}$ oligomers, one set of cultures received hiPSC-NSC-EVs (6×10^9 EVs). The dose of hiPSC-NSC-EVs employed in the study was based on a parallel study in our laboratory, which demonstrated that 6×10^9 hiPSC-NSC-EVs are adequate to provide significant neuroprotection to human neurons exposed to 1 μM $\text{A}\beta_{42}$ oligomers. The hiPSC-NSC-EVs were added 4 h after $\text{A}\beta_{42}$ oligomers exposure to determine whether EVs could protect iMicroglia from becoming activated iMicroglia following exposure to $\text{A}\beta_{42}$ oligomers. Twenty hours later, iMicroglia from all culture sets were, dissociated, collected, washed, and processed for total RNA isolation and quantitative real-time PCR (qPCR) studies. We performed another set of experiments to understand potential changes in the phagocytic ability of iMicroglia after $\text{A}\beta_{42}$ exposure with or without EV treatment. Twenty-three hours after $\text{A}\beta_{42}$ exposure, fluorescent yellow-green latex beads (Sigma-Aldrich) were added to iMicroglia cultures treated with or without EVs. One hour later, images were captured, and the percentages of iMicroglia incorporating latex beads were quantified.

2.6 | Analyses of cognitive and mood function using neurobehavioral tests

Both male and female mice in naïve, AD-Veh, and AD-EVs groups were investigated with two neurobehavioral tests to measure cognitive function. The behavioural tests commenced 3 weeks after Veh/EVs administration and continued for a month (i.e., in the 5th month of life). Although EVs incorporate into microglia and encounter astrocyte/astrocyte processes rapidly (Attaluri et al., 2023), we reasoned that modulation of inflammatory pathways, and the impact of such modulation would take at least a couple of weeks to culminate in beneficial effects on cognitive function. Therefore, we commenced behavioural studies 3 weeks after the second administration of EVs. An object location test (OLT) ascertained the proficiency of animals to discern minor changes in their immediate environment, a cognitive function entirely dependent on the hippocampus (Warburton & Brown, 2015). A pattern separation test (PST) ascertained the competence of animals to distinguish similar but not identical experiences in a nonoverlapping manner (Jain et al., 2012), a measure of pattern separation ability dependent on the dentate gyrus (DG) function. A sucrose preference test (SPT) assessed mood function by examining anhedonia or depressive-like behaviour. The detailed protocols employed for OLT, PST, and SPT are available in our previous reports (Kodali et al., 2023a; Long et al., 2017; Shetty et al., 2020; Upadhyaya et al., 2019) and the [supplementary file](#).

2.7 | Harvesting of brain tissues for immunohistochemical and molecular assays

The animals in all groups were euthanized following neurobehavioral tests when they were 5 months old. Fixed brain tissues were obtained for immunohistochemical studies, and fresh brain tissues were harvested for molecular assays. The details on the harvesting and processing of fixed and fresh tissues for immunohistochemical and molecular analyses are available in our published studies (Ayyubova et al., 2023; Long et al., 2017; Madhu et al., 2019, 2021; Rao et al., 2008; Shetty et al., 2020) and the [supplementary file](#).

2.8 | Quantification of numbers, clusters and proliferation of microglia, macrophage infiltration, and $\text{A}\beta_{42}$ plaques

The numbers of microglia were quantified in the hippocampus of male and female naïve, AD-Veh, and AD-EVs groups via stereological counting of Ionized calcium-binding adaptor molecule 1 (IBA1+) cells through the entire hippocampus in serial sections (every 20th section) from naïve, AD-Veh, and AD-EVs groups ($n = 6/\text{group}$), as described in our previous reports (Ayyubova et al., 2023). We also quantified the number of microglial clusters per cubic millimetre (mm^3) volume from different hippocampal subfields in male and female AD mice receiving Veh or EVs. Image J was employed to quantify the extent of $\text{A}\beta$ plaques in the hippocampus. The percentage of proliferating microglia was quantified in male AD mice receiving Veh or EVs through IBA-1 and Ki67 dual immunofluorescence and Z-section analysis in a confocal microscope ($n = 5/\text{group}$). The percentage of IBA1+ cells lacking microglia-specific transmembrane protein 119 (TMEM119) expression (i.e., macrophages, Jurga et al., 2020) were quantified in male and female AD mice receiving Veh or EVs to assess the extent of macrophage infiltration ($n = 5/\text{group}$).

2.9 | Quantification of astrocyte hypertrophy

The hypertrophy of astrocytes in the dentate gyrus (DG) and hippocampal CA1 and CA3 subfields was evaluated by measuring area fractions occupied by glial fibrillary acidic protein (GFAP) immunoreactive structures using Image J (4 sections/subfield/animal, $n = 5\text{--}6/\text{group}$), as described in our previous report (Ayyubova et al., 2023).

2.10 | Isolation of RNA from iMicroglia and mouse hippocampus for qPCR studies

Total RNA isolation kits were employed to isolate RNA from cultured iMicroglia ($n = 4/\text{group}$; System Bioscience, Palo Alto, CA, USA) and the mouse hippocampal tissues ($n = 5\text{--}6/\text{group}$; Qiagen, Germantown, MD, USA). The samples of the RNA (500 ng/ μL) were converted into cDNA using RT2 First Strand Kit (Qiagen). The qRT-PCR was performed using RT² SYBR Green qPCR Mastermix and Primer mix (GeneCopoeia, Rockville, Maryland, USA) for measuring human microglial gene expression in iMicroglia such as *tmem119*, *purinergic receptor P2Y12 (p2ry12)*, *cluster of differentiation 68 (cd68)*, *CX3C motif chemokine receptor 1 (cx3cr1)*, *complement 1qa (clqa)*, *cystatin-7 (cst7)*, *cathepsin D (ctsd)*, *apolipoprotein E (apoe)*, *lipoprotein lipase (lpl)*, *ferritin heavy chain 1 (fth1)*, *interleukin 1 beta (il1b)*, *tumor necrosis factor alpha (tnfa)* and mouse microglial gene expression in the hippocampus (*cst7*), *secreted phosphoprotein 1 (spp1)*, *lpl*, *apoe*, *fth1*, *TYRO protein tyrosine kinase-binding protein (tyrobp)*, *triggering receptor expressed on myeloid cells 2 (trem2)*, *ctsd*, *nlrp3*, *PYD*, and *CARD domain-containing protein (pycard)*, *caspase 1 (caspl)*, *il1b*, and *il18*. The details of primers employed in the study are detailed in the Supplementary file (Table S1).

2.11 | Measurement of NLRP3 inflammasome complexes in microglia

The brain tissue sections were processed for triple immunofluorescence staining and Z-section analysis using a Nikon confocal microscope or Leica THUNDER 3D Imager for measuring the percentages of microglia displaying NLRP3 inflammasome complexes (i.e., cells positive for IBA-1, NLRP3, and apoptosis-associated speck-like protein containing a caspase recruitment domain (ASC) in the hippocampus (Ayyubova et al., 2023). All measurements were performed in the CA3 subfield of the hippocampus (3 sections/animal, $n = 6/\text{group}$). The methods and antibodies employed for these studies are described in the [supplementary file](#).

2.12 | Quantification of mediators and end products of NLRP3 inflammasome activation

The mediators and proinflammatory end products of NLRP3 inflammasome activation were quantified from hippocampal tissue lysates using ELISA ($n = 6/\text{group}$), as detailed in our previous study (Madhu et al., 2021). Commercially available kits for measuring nuclear factor kappa B (NF- κB , Aviva Systems Biology, San Diego, CA, USA), NLRP3 (Abcam, Cambridge, MA, USA), ASC (MyBioSource, San Diego, CA, USA), cleaved caspase-1 (BioVision Inc, Milpitas, CA, USA), interleukin-18 (IL-18), IL-1 β (R&D Systems, Minneapolis, MN, USA) were utilized.

2.13 | Measurement of proteins linked to hyperactivation of p38/MAPK, interferon signalling cascade, and double-stranded DNA fragments (dsDNA) accumulation within microglia

The hippocampal tissue lysates were utilized for quantifying the various markers involved in IL-18-mediated hyperactivation of the p38/MAPK signalling pathway and its proinflammatory end products ($n = 6/\text{group}$). We followed the manufacturer's protocol provided in individual ELISA kits for the myeloid differentiation primary response 88 (MyD88, Aviva Systems Biology), small GTPase rat sarcoma virus (Ras, MyBioSource), p38 MAPK (Cell Signalling, Danvers, MA, USA), activator protein-1 (AP-1, Novus Biologicals, Centennial, CO; USA), IL-6, tumour necrosis factor- α (TNF α , R&D systems), IL-8 (Biomatik, Wilmington, DE, USA) and macrophage inflammatory protein-1 alpha (Mip-1 α , Signosis, Santa Clara, CA, USA). The concentrations of these individual proteins were normalized to the 1 mg of total protein in hippocampal lysates, and values were compared across groups. Furthermore, we also measured cGAS, p-STING, phosphorylated interferon regulatory factor 3 (p-IRF3), and IFN- α concentrations in the hippocampus. Additionally, we processed the brain tissue sections for dual immunofluorescence staining for IBA-1 and dsDNA to measure the percentage of microglia containing dsDNA in their cytoplasm, as described elsewhere (Li et al., 2020). Next, Z-section analysis in a Nikon confocal microscope measured the percentages of microglia displaying dsDNA (i.e., cells positive for IBA-1 and dsDNA) in the CA1 subregion of the hippocampus. (3 sections/animal, $n = 5/\text{group}$). The methods and antibodies employed for these studies are described in the [Supplementary File](#).

2.14 | Quantification of A β 42 and p-tau concentrations

The five FAD mutations in 5xFAD mice lead to A β 42 overproduction and increased Ser396 tau phosphorylation (Kanno et al., 2014). Therefore, we measured the concentrations of A β 42 and p-tau in the hippocampal tissue lysates of naïve, AD-Veh, and AD-EVs groups. We followed the manufacturer's protocol described in ELISA kits for measuring A β 42 (Invitrogen, Waltham,

MA, USA) and p-tau (Cell Signalling, Danvers, MA, USA). The concentrations of A β 42 and p-tau were normalized to mg of protein in hippocampal lysates.

2.15 | Measurement of microglial phagocytosis in vivo using A β 42 labelling

We performed intraperitoneal injection of methoxy-X04 (m-X04; 10 mg/kg) to ascertain the phagocytotic activity of microglia in AD-Veh and AD-EVs groups ($n = 5$ /group) in the 5th month of life (i.e., ~2 months after Veh/EVs treatment). Three hours later, the mice were deeply anesthetized, and brain tissues were fixed via intracardiac perfusions using 4% paraformaldehyde. The brain tissue sections were processed for dual immunofluorescence methods to visualize IBA-1 and A β . Next, we measured the percentages of microglia internalizing m-X04-bound A β (Lau et al., 2021) through Z-section analysis in a Nikon confocal microscope.

2.16 | Statistical analyses

Statistical analyses of data utilized Prism software 10.1. Within-group comparisons in neurobehavioral tests or two-group comparisons utilized a two-tailed, unpaired Student's *t*-test or Mann–Whitney *U*-test for two datasets with significantly different standard deviations. All comparisons involving three or more datasets were analysed using one-way ANOVA with Tukey's multiple comparisons post-hoc tests. However, when individual groups did not pass the normality test (Shapiro–Wilk test), Kruskal–Wallis test with Dunn's post hoc tests were performed. The discrimination index (DI) values in neurobehavioral tests were compared to the hypothetical mean (zero) using a one-sample *t*-test (Contreras et al., 2024). In all comparisons, $p < 0.05$ was considered a statistically significant value. We also performed two-way ANOVA with Tukey's multiple comparisons post-hoc tests to determine sex-dependent effects and the interaction between sex and hiPSC-NSC-EVs treatment.

3 | RESULTS

3.1 | hiPSC-NSC-EVs displayed EV-specific markers and ultrastructure and were internalized by microglia in 5xFAD mouse brain following IN administration

The hiPSC-NSC-EVs were small EVs (30–250 nm in diameter, average size = 145 nm; Figure S1(A)). They expressed multiple EV-specific markers, including CD63, CD81, and Alix, and lacked cytoplasmic markers expressed in parental NSCs such as calnexin and cytochrome C (Figure S1(B)). Transmission electron microscopy revealed vesicles displaying double membrane (Figure S1(C)). The miRNA and protein composition of these hiPSC-NSC-EVs have been described in our previous study (Upadhyaya et al., 2020). The ability of IN-administered EVs to incorporate into neurons and microglia and encounter astrocyte soma and processes in all brain regions of the 5xFAD mice has been presented in our recent study (Attaluri et al., 2023). Microglia in virtually all forebrain regions of 5xFAD mice, including PAM, internalized IN administered PKH-26+ EVs when examined 45 min post-administration (Figure S2(A–H)). Although neurons and astrocytes are the significant sources of A β production (Frost & Li, 2017; Huffels et al., 2023), A β plaques accumulating in extracellular spaces were consistently covered by microglia (i.e., PAM). Confocal imaging demonstrated that A β plaques were always surrounded by microglia and astrocytes. Furthermore, plaques surrounded by microglia and astrocytes could be seen both adjacent and away from hippocampal neuronal cell layers in 5xFAD mice (Figure S3).

3.2 | hiPSC-NSC-EV incorporation triggered transcriptomic changes within microglia of 5xFAD mice

Figure S4 outlines the experimental design employed in the study. First, we investigated transcriptomic changes in microglia induced by hiPSC-NSC-EVs at 72 h post-administration using the scRNA seq. The pattern of t-SNE plot of microglia from the AD-Veh group differed from corresponding plots from naïve and AD-EVs groups (Figure 1(a)). The AD-Veh group showed upregulation of 8735 genes and downregulation of 1300 genes vis-à-vis the naïve group. In contrast, the AD-EVs group demonstrated upregulation of 4050 genes and downregulation of 1402 genes compared to the naïve group. Compared to the AD-Veh group, the AD-EVs group displayed upregulation of 1506 genes and downregulation of 8280 genes (Figure 1(b)), Figure S5). Microglia with a high DAM gene signature were apparent in the AD-Veh group compared to the naïve group (Figure 1(c–d)). The upregulated genes comprised *ctsd*, *ctsb*, *ctsl*, *ctsz*, *axl* receptor tyrosine kinase (*axl*), *glycoprotein nonmetastatic melanoma protein*

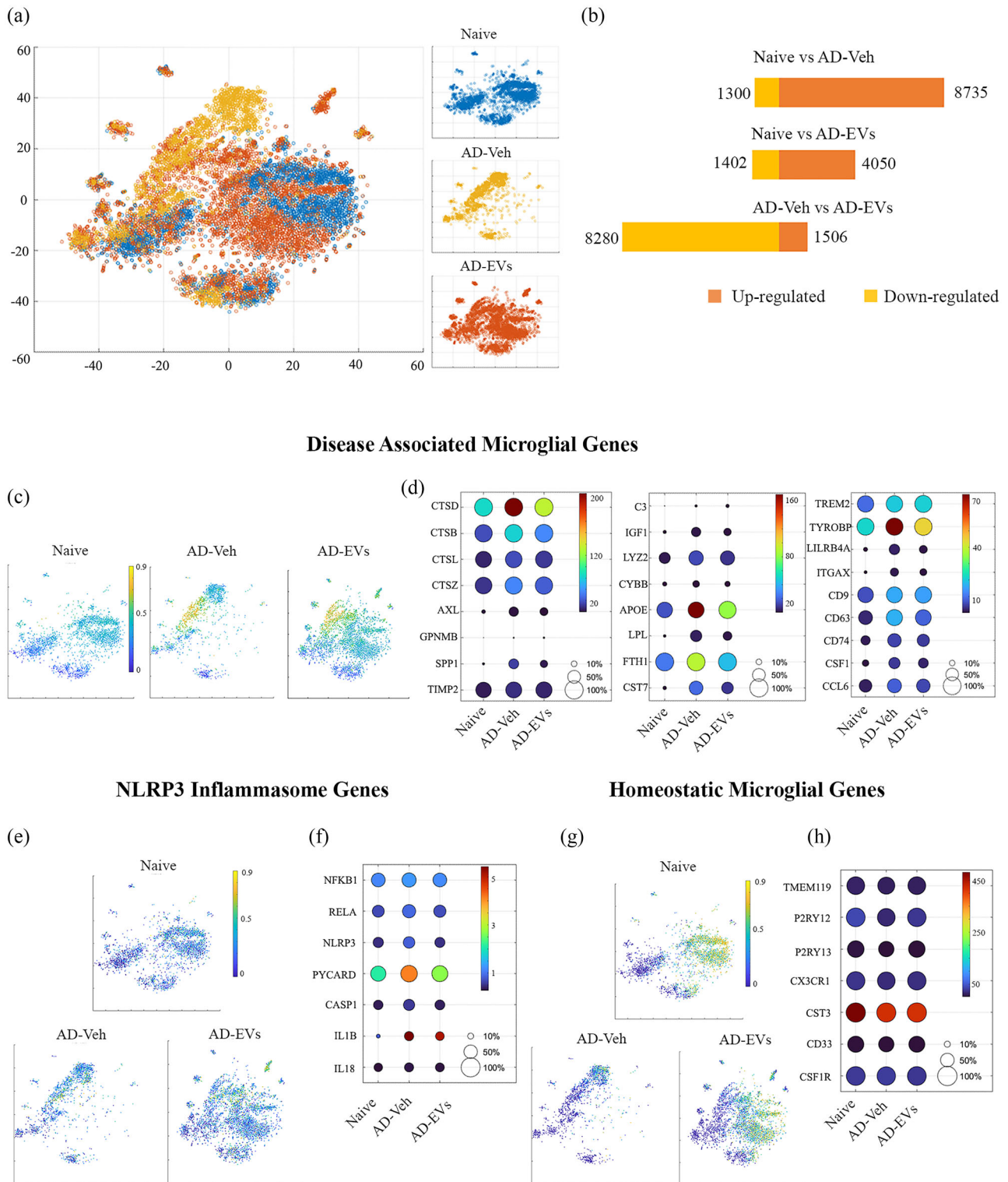


FIGURE 1 Intranasal administration of extracellular vesicles from human induced pluripotent stem cell-derived neural stem cells (hiPSC-NSC-EVs) altered the expression of genes linked to disease-associated microglia (DAM) and NOD-, LRR-, and pyrin domain-containing protein 3 (NLRP3) inflammasome activation in 5xFAD mice microglia when observed 72 h post-EVs administration. Figure (a) illustrates the distinct t-SNE plots of microglia in naive, AD-Veh, and AD-EVs groups. (b) represents the total number of microglial genes upregulated and downregulated in the AD-Veh and AD-EVs groups compared to the naive group. (c and d) represent the Ucell score scatter plot and dot plots of different DAM genes in microglia of naive, AD-Veh, and AD-EVs groups. (e and f) represent the Ucell score scatter plot and dot plots of different NLRP3 inflammasome genes in microglia of different groups. (g and h) represent the Ucell score scatter plot and dot plots of different homeostatic microglial genes in microglia of different groups.

B (*gpnmb*), *spp1*, *tissue inhibitor of metalloproteinase (timp2)*, *c3*, *insulin like growth factor 1 (igf1)*, *lysozyme 2 (lyz2)*, *cytochrome B beta chain (cybb)*, *apoe*, *lpl*, *fth1*, *cst7*, *trem2*, *tyrobp*, *leukocyte immunoglobulin-like receptor, subfamily B, member 4A (lilrb4a)*, *integrin subunit alpha X (itgax)*, *cd9*, *cd63*, *cd74*, *colony stimulating factor 1 (csf1)*, *chemokine ligand 6 (ccl6)*. Notably, most of these genes, except *gpnmb*, *c3*, *trem2*, *cd9* were downregulated in the AD-EVs group, compared to AD-Veh group (Figure 1(c-d), Figure S6(A)). Furthermore, multiple genes linked to NLRP3 inflammasomes (*nuclear factor kappa B; nfkb1*, *NF-kappa-B transcription factor P65 (rela)*, *nlrp3*, *pycard*, *caspl*, *illb*, *ill8*) were upregulated in the AD-Veh group. The expression of many of these genes (*rela*, *nlrp3*, *pycard*, *caspl*, *illb*) was reduced in the AD-EVs group (Figure 1(e-f), Figure S6(B)). Moreover, the expression of microglial homeostatic genes (*p2ry12*, *p2ry13*, *cx3cr1*, and *cd33*) was downregulated in the AD-Veh group but normalized in the AD-EVs group (Figure 1(g-h)). Furthermore, the AD-Veh group displayed upregulation of multiple genes linked to the signalling of IFN-1 (18 genes), IFN- γ (27 genes), and IL-6 (23 genes). The AD-EVs group displayed normalized or reduced expression of many upregulated genes related to these signalling pathways. These include genes beta-2-microglobulin (*b2m*), *bone marrow stromal cell antigen 2 (bst2)*, *guanylate binding protein 3 (gbp3)*, *gbp7*, *histocompatibility 2, K1 (h2-k1)*, *Interferon Induced transmembrane protein 3 (ifitm3)*, *galectin 3 binding protein (lgals3bp)*, *proteasome 20S subunit beta 8 (psmb8)*, *psmb10*, *ring finger protein 2 (rnf2)*, *signal transducer and activator of transcription (stat1)*, *stat2*, *transporter 2, ATP binding cassette subfamily B member (tap2)* and *tap binding protein (tapbp)* (IFN-1 signalling genes), *cd86*, *cd274*, *Fc gamma receptor 1 (fcgr1)*, *homeostatic iron regulator (hfe)*, *janus kinase 2 (jak2)*, *psmb9*, *stat1* (IFN- γ signalling genes), and *cd14*, *cytokine receptor like factor 2 (crlf2)*, *csf1*, *colony stimulating factor 2 receptor subunit beta (csf2rb)*, *csf3r*, *interferon alpha receptor 1 (ifnar1)*, *interferon gamma receptor 2 (ifngr2)*, *illb*, *il10rb*, *il13Ra1*, *il15ra*, *IL17ra*, *ltbr*, *myd88*, *protein tyrosine phosphatase non-receptor type 2 (ptpn2)*, *suppressor of cytokine signalling 3 (socs3)*, *stat1*, *stat2*, *stat3*, *toll like receptor 2 (tlr2)*, and *tnf* (IL-6 signalling genes) (Figure 2 and Figures S7–S9).

Additional analysis on astrocyte cell populations revealed no batch effect as shown in the t-SNE plot, where cells from the AD-Veh group overlapped with those from naïve and AD-EVs groups (Figure S10). Despite of this global similarity across groups, the expression of multiple genes linked to IFN-1 signalling (*b2m*, *HECT*, and *RLD domain containing E3 ubiquitin protein ligase family member 6 (herc6)*, *interferon induced transmembrane protein 3 (ifitm3)*, *interferon gamma induced GTPase (igtp)*, *immunity related GTPase M 1 (irgm1)*, *lgals3bp*, *rnf2*, *radical S-adenosyl methionine domain containing 2 (rsad2)*, *stat1*, *stat2*, *tapbp*) and IL-6 signalling (*cd9*, *csf1*, *ifnar1*, *ifngr1*, *il10rb*, *il15ra*, *il6st*, *ptpn2*, *stat1*, *stat2*, *stat3*) was upregulated in astrocytes from the AD-Veh group compared to astrocytes in the naïve group. Notably, the expression of these genes was significantly reduced in the AD-EVs group (Figures S10–S11). Thus, IN-administration of hiPSC-NSC-EVs in 5xFAD mice resulted in significant transcriptomic changes in microglia and astrocytes, implying alleviation of increased NLRP3, IFN-1, IFN- γ , and IL-6 signalling.

3.3 | hiPSC-NSC-EVs treatment reduced A β 42-induced activation of cultured human iMicroglia

We next examined whether hiPSC-NSC-EVs are also proficient in moderating the expression of genes in cultured human iMicroglia challenged with A β 42 oligomers. iMicroglia, generated from hiPSCs and expressing the microglia-specific TMEM119 (Figure 3(a-e)), were exposed to A β 42 (1 μ M) for 24 h. One set of cultures received 6×10^9 hiPSC-NSC-EVs at 4 h after A β 42 exposure (Figure 3(f)). The expression of homeostatic microglia genes (*tmem119*, *p2ry12*) did not differ between naïve, A β 42-exposed, and A β 42-exposed and hiPSC-NSC-EV treated iMicroglia ($p > 0.05$; Figure 3(g-h)). However, compared to the naïve iMicroglia, the expression of multiple genes linked to microglia activation (*cd68*, *cx3cr1*, *clqa*), DAM (*ctsd*, *apoe*, *lpl*, *fth1*) and inflammation (*illb*, *tnfa*) were upregulated in the A β 42-exposed iMicroglia ($p < 0.05$ – 0.01 , Figure 3(i-r)) but not in the A β 42-exposed iMicroglia treated with hiPSC-NSC-EVs ($p > 0.05$, Figure 3(i-r)). Investigation of phagocytosis function revealed that hiPSC-NSC-EVs mediated reduced activation of iMicroglia did not interfere with their phagocytosis function (Figure S12). Thus, hiPSC-NSC-EVs can also moderate human microglial activation without compromising their phagocytosis function.

3.4 | hiPSC-NSC-EV administration preserved cognitive, memory, and mood function at 5 months of age

We first measured the competence of animals to recognize minor changes in the immediate environment, a hippocampus-dependent cognitive function, using an OLT (Figure 4a). Most of the animals (10–13 males and 6–13 females) met the criteria employed for this task (i.e., exploration of objects ≥ 20 s in trial-2 (T2)). Proficiency for object location memory was intact in both males and females in the age-matched naïve control group when analysed separately or together ($p < 0.01$ – 0.0001 ; Figure 4(b,f,j)), but was impaired in both males and females in the AD-Veh group ($p > 0.05$, Figure 4(c,g,k)). Contrastingly, both males and females in the AD-EVs group displayed no cognitive impairment ($p < 0.05$ – 0.001 , Figure 4(d,h,l)). Intact cognitive function in naïve and AD-EV groups was evident from the propensity of animals to explore the object in novel place (OINP) for longer durations than the object in familiar place (OIFP). Analysis of the OINP-DI values using a one-sample t-test revealed proficiency for the cognitive task in the naïve group (males and females, alone or together, $p < 0.05$ – 0.01) and the AD-EVs group (males, $p < 0.05$, both sexes, $p < 0.01$) but not in the AD-Veh group (Figure 4(e,i,m)). The results were not influenced by variable

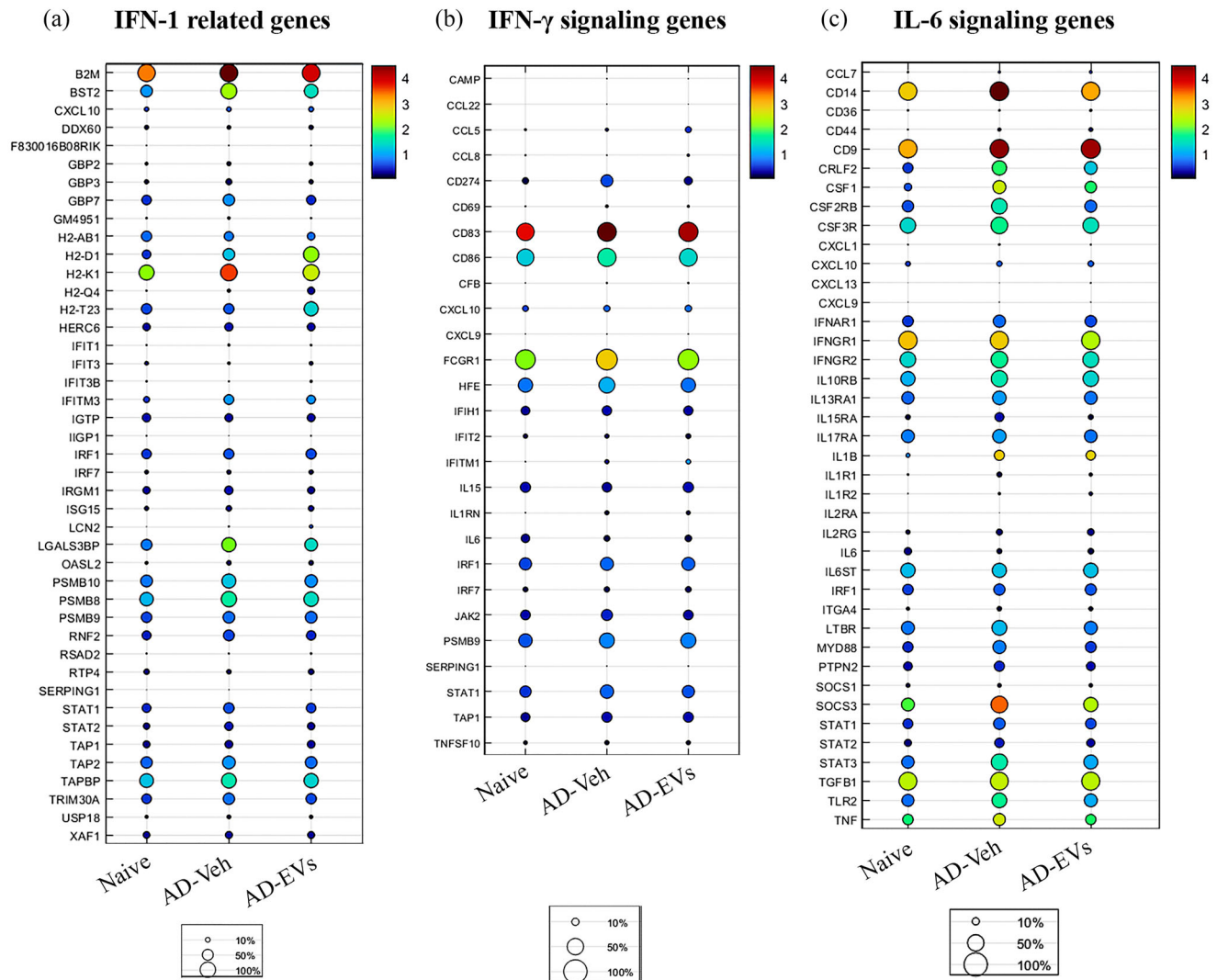


FIGURE 2 Intranasal administration of extracellular vesicles from human induced pluripotent stem cell-derived neural stem cells (hiPSC-NS-EVs) altered the expression of genes linked to interferon-1 (IFN-1), interferon-gamma (IFN- γ) interleukin-6 (IL-6) signalling in 5xFAD mice microglia when observed 72 h post-EVs administration. Dot plots in A-C compare the expression of multiple genes linked to IFN-1, IFN- γ signalling, and IL-6 signalling pathways between naive, AD-Veh, and AD-EVs groups. The expression of most genes was upregulated in the AD-Veh group compared to the naive group but reduced in the AD-EVs treatment group compared to the AD-Veh group.

object exploratory behaviour between groups, as the total object exploration times (TOETs) in T2 did not differ between groups ($p > 0.05$, Figure S13(A-B)).

Next, we determined the pattern separation ability of animals using a PST (Figure 4(n)), which examined the proficiency for discriminating the novel object (NO) from the familiar object (FO) kept on a second-floor pattern (P2) in T4 of PST. Most animals (9–11 males and 9–12 females) in every group met the criteria (i.e., exploration of objects ≥ 20 s in T2 and T3). Adeptness for recognizing the NO on P2 in T4 was intact in both males and females in the naive ($p < 0.0001$, Figure 4(o,s,w)) and AD-EVs ($p < 0.01$ – 0.0001 , Figure 4(q,u,y)) groups but impaired in the AD-Veh group ($p > 0.05$, Figure 4(p,t,x)). Proficiency for pattern separation in naive and AD-EV groups was evident from the propensity of animals to explore the NO on P2 for longer durations than the FO on P2. Analysis of the NO on P2-DI values using a one-sample t-test confirmed competence for pattern separation in males and females of the naive group ($p < 0.01$ – 0.0001) and the AD-EVs group ($p < 0.05$ – 0.01) but not in the AD-Veh group (Figure 4(r,v,z)). As observed in OLT, the findings were not prompted by varying object exploratory behaviour between groups, as the TOETs in T2 and T3 did not differ between groups ($p > 0.05$, Figure S13(C-F)).

Furthermore, an investigation of mood function using a SPT ($n = 10$ – 11 males and 9–10 females per group, Figure 5(a)) revealed anhedonia in the AD-Veh group compared to the naive group but not in the AD-EVs group (Figure S13(G-L)). Absence of anhedonia in both sexes in naive and AD-EVs groups was evident from the preference of animals to drink higher amounts of sucrose-containing water than standard water ($p < 0.0001$, Figure S13 (G, I, J, L)). In contrast, the presence of anhedonia in

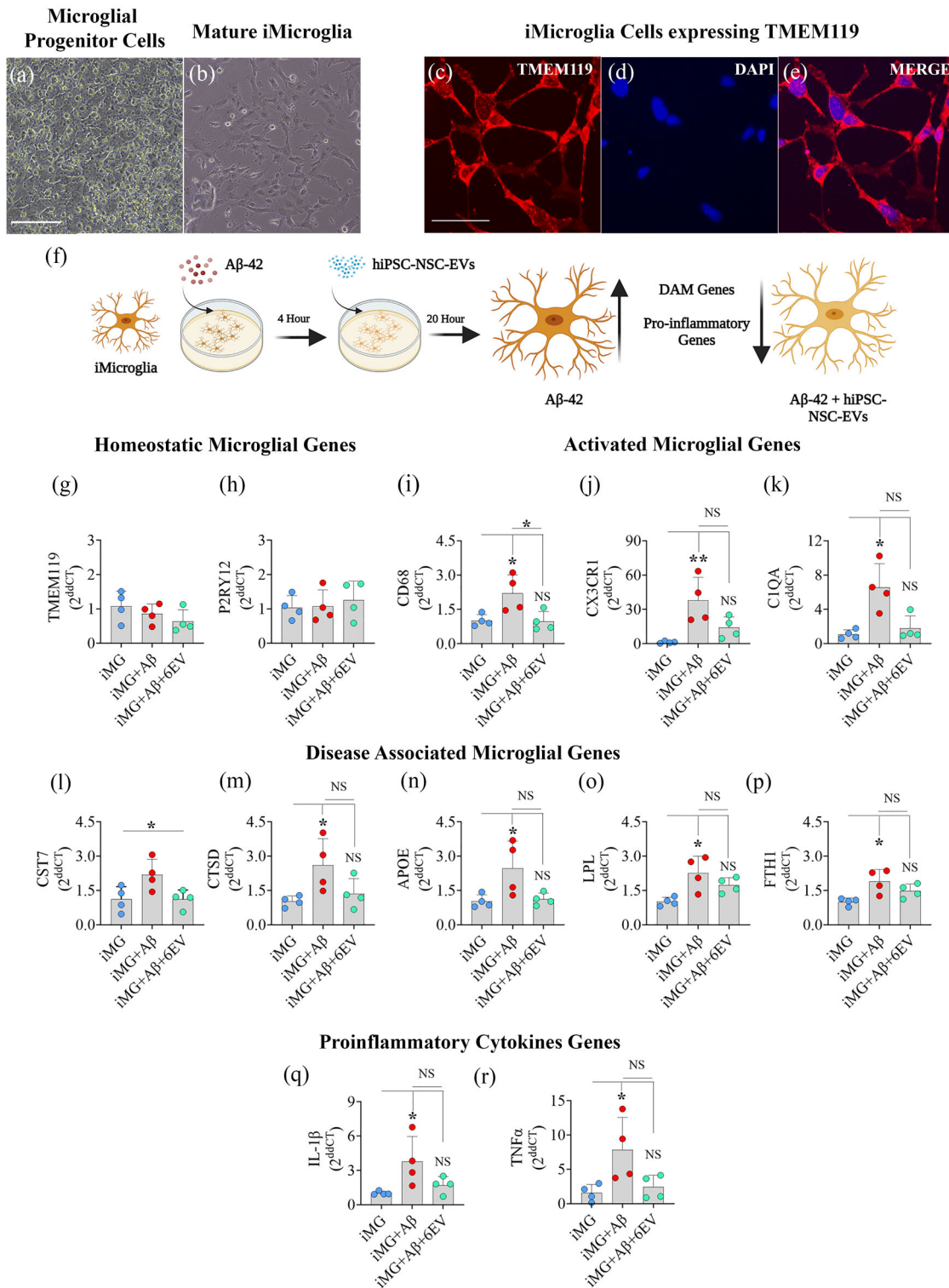
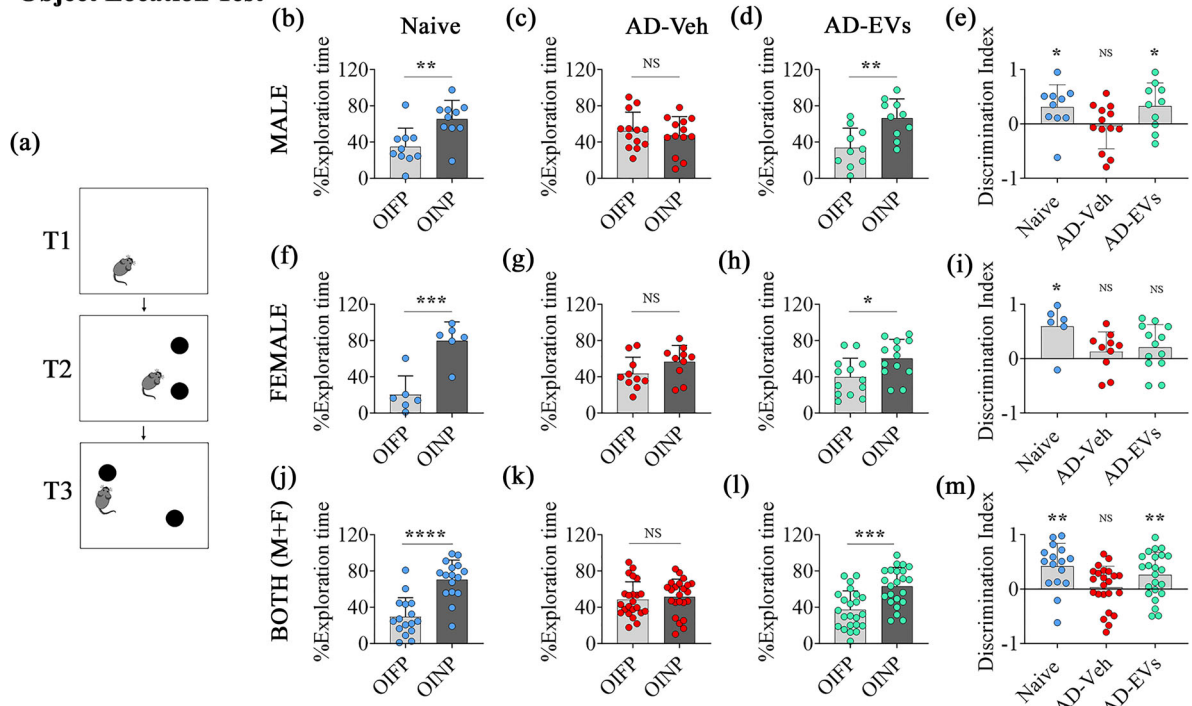


FIGURE 3 Intranasal administration of extracellular vesicles from human induced pluripotent stem cell-derived neural stem cells (hiPSC-NSC-EVs) suppressed Aβ42-induced activation of iMicroglia derived from hiPSCs. Images (a and b) show the progenitor and mature microglia from hiPSCs. (c-e) images confirm TMEM119 expression in mature microglia. (f) is a diagrammatic representation of the experiment involving Aβ42 exposure to iMicroglia followed by hiPSC-NSC-EV treatment. Bar charts (g-h), (i-k), (l-p), and (q-r) respectively compare the expression of homeostatic genes (g-h), activated microglia genes (i-k), disease-associated microglia (DAM) genes (l-p), and proinflammatory cytokine genes (q-r) in iMicroglia between control, Aβ42-exposed, and Aβ42-exposed and hiPSC-NSC-EVs treated cultures. Scale bar, A-E = 100 μm; *, $p < 0.05$; **, $p < 0.01$; NS, not significant.

Object Location Test



Pattern Separation Test

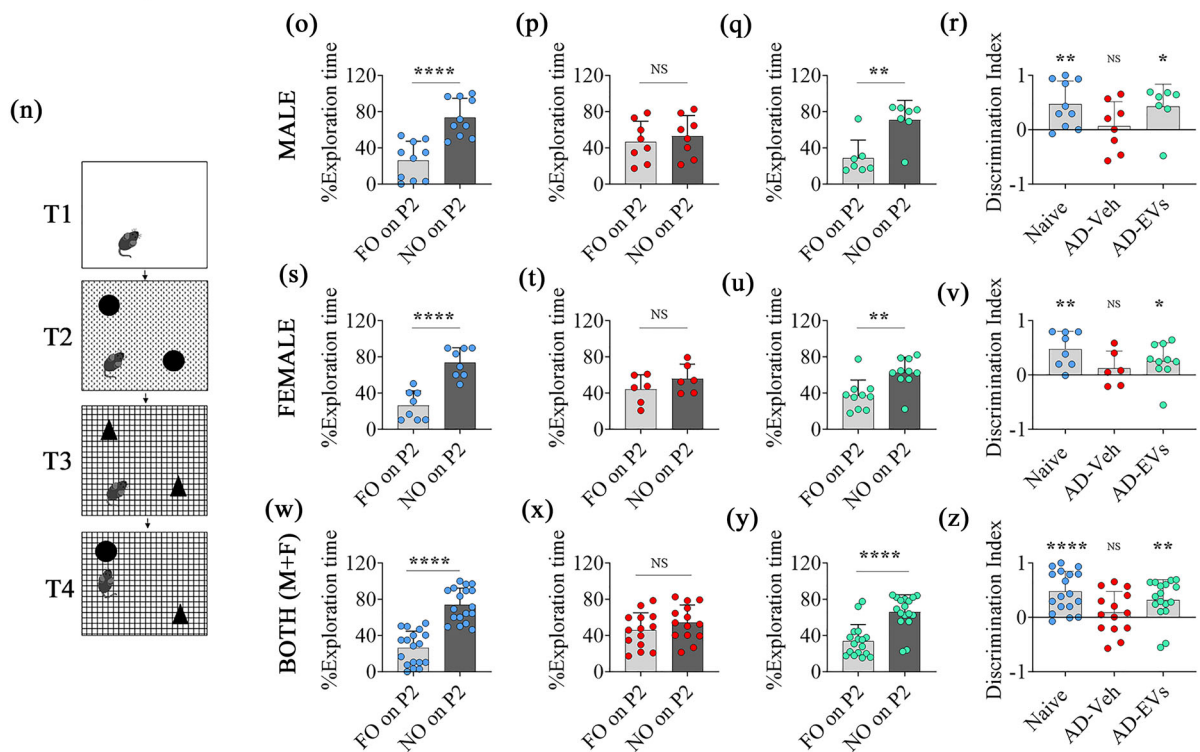


FIGURE 4 Intranasal administration of extracellular vesicles from human induced pluripotent stem cell-derived neural stem cells (hiPSC-NSC-EVs) to 5xFAD mice preserved cognitive function. Cartoon A depicts different trials (t1-t3) in an object location test (OLT). The bar charts in b-d, f-h, j-l compare percentages of object exploration times spent with the object in the familiar place (OIFP) vis-à-vis the object in the novel place (OINP) in naïve (b, f, j), AD-Veh (c, g, k), and AD-EVs (d, h, l) in males (b-d), females (f-h), and when both males and females were considered together (j-l). The bar charts e, i, m compare the OINP discrimination index (DI) for males (e), females (i), and both sexes (m) using a one-sample *t*-test. Cartoon N depicts different trials (t1-t4) in a pattern separation test (PST). The bar charts in o-q, s-u, w-y compare percentages of object exploration times spent with the familiar object on pattern 2 (FO on P2) vis-à-vis the novel object on P2 (NO on P2) in naïve (o, s, w), AD-Veh (p, t, x), and AD-EVs (q, u, y) in males (o-q), females (s-u) when both males and females were considered together (W-Y) together. The bar charts R, V, Z compare the DI for the NO on P2 for males (r), females (v), and both sexes (z) using a one-sample *t*-test. *, $p < 0.05$; **, $p < 0.01$; ***, $p < 0.001$; and ****, $p < 0.0001$; NS, not significant.

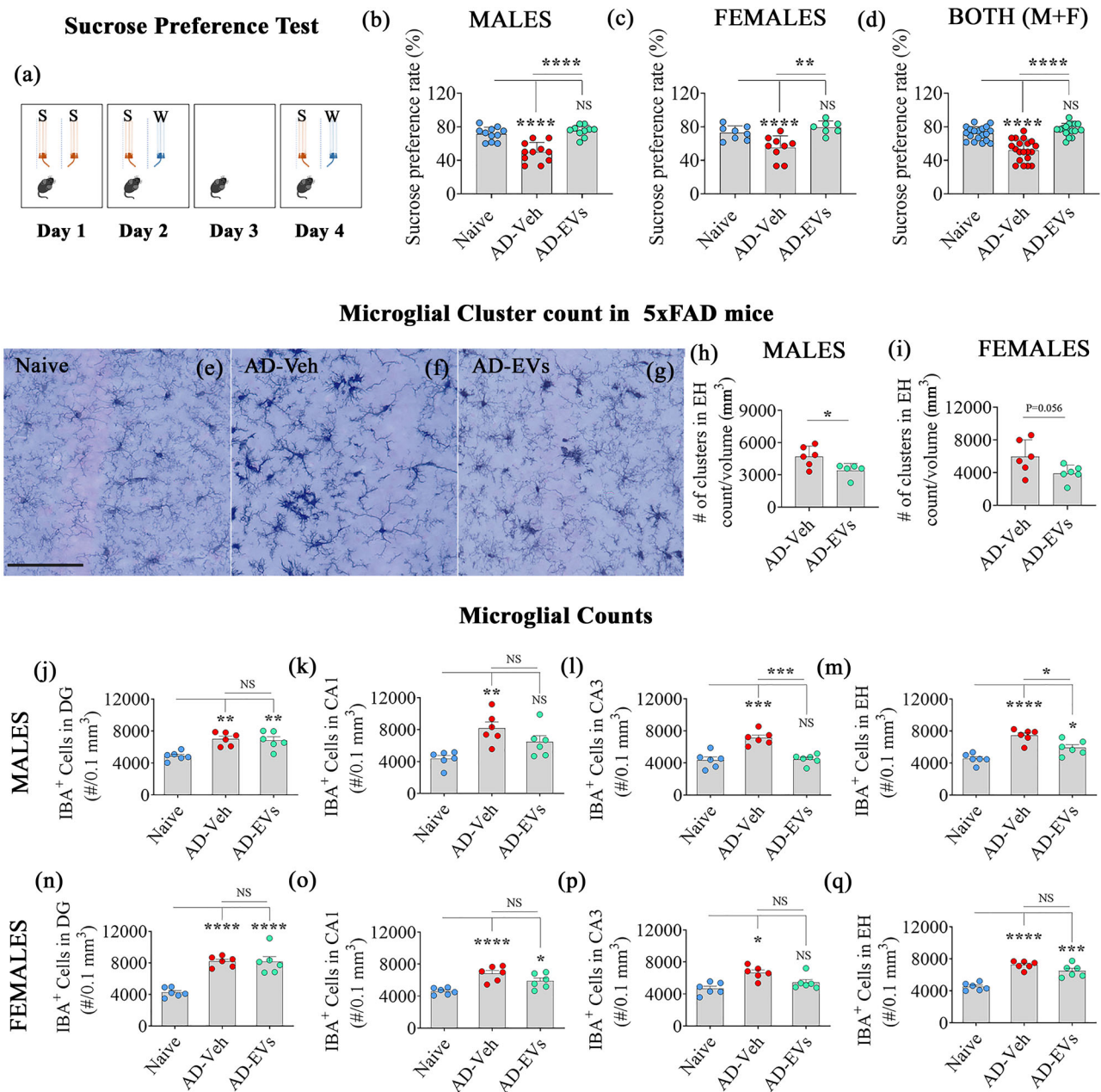


FIGURE 5 Intranasal administration of extracellular vesicles from human induced pluripotent stem cell-derived neural stem cells (hiPSC-NSC-EVs) to 5xFAD mice prevented anhedonia and reduced microglial clusters and numbers. Cartoon (A) depicts the experimental design employed for the sucrose preference test. The bar charts (B-D) compare the sucrose preference rate (SPR) in males (B), females (C) and males + females (D) across naïve, AD-Veh and AD-EVs groups. **, $p < 0.01$; ****, $p < 0.0001$; NS, not significant. Figure (E-G) illustrates the representative images of microglial clusters in naïve (E), AD-Veh (F), and AD-EVs (G) groups. Bar charts (H-I) compare the number of microglial clusters per mm³ unit area of the hippocampus in males (H) and females (I) between naïve, AD-Veh, and AD-EVs groups. Bar charts J-Q compare numbers of microglia in males (J-M) and females (N-Q) per 0.1 mm³ area of the dentate gyrus (J, N), CA1 subfield (K, O), CA3 subfield (L, P), and the entire hippocampus (M, Q) between naïve, AD-Veh, and AD-EVs groups. Scale bar, E-G = 100 μm *, $p < 0.05$; **, $p < 0.01$; ***, $p < 0.001$; ****, $p < 0.0001$; NS, not significant.

both sexes in the AD-Veh group was apparent from the lack of preference of animals to drink sweet water ($p > 0.05$, Figure S13 (H, K)). Comparison of the sucrose preference rate (SPR) across groups confirmed differences between naïve and AD-Veh groups, and between AD-Veh and AD-EVs groups, for both males and females or when both sexes were considered together ($p < 0.01$ – 0.0001 , Figure 5(b,c,d)).

Thus, hiPSC-NSC-EVs intervention at 3 months of age in male and female 5xFAD mice prevented the occurrence of cognitive and mood impairments at 5 months of age. Additional two-way ANOVA analysis revealed no sex-dependent differences or interactions between sex and hiPSC-NSC-EVs treatment for the OLT, PST, and SPT in 5xFAD mice (Table S2).

3.5 | hiPSC-NSC-EVs administration reduced microglial clusters and numbers in the hippocampus

We quantified the number of microglial clusters in different hippocampal subfields (Figure 5(e-i)). IBA-1+ microglial clusters, were conspicuous in all hippocampal subfields in AD-Veh and AD-EVs groups. However, males in the AD-EVs group displayed a reduced number of microglial clusters per mm³ compared to the AD-Veh group ($p < 0.05$, Figure 5(h)). The females in the AD-EVs group also showed a similar trend, but the difference was not significant ($p = 0.056$, Figure 5(i)). Furthermore, in both sexes, compared to the naïve group, the AD-Veh group displayed an increased number of microglia in all subfields and the entire hippocampus ($p < 0.05$ – 0.0001 , Figure 5(j-q)). Males in the AD-EVs group exhibited reduced numbers of microglia in the CA3 subfield and the entire hippocampus compared to the AD-Veh group ($p < 0.05$ – 0.001 ; Figure 5(l,m)). However, females in the AD-EVs group displayed similar numbers of microglia as the AD-Veh group in all hippocampal subfields (Figure 5(n-q)). Thus, hiPSC-NSC-EV treatment reduced microglial clusters and numbers in male 5xFAD mice. The females showed a similar trend, but the reductions were not statistically significant. Notably, two-way ANOVA analysis revealed no sex-dependent differences or interactions between sex and hiPSC-NSC-EVs treatment for microglial clusters and counts in 5xFAD mice (Table S2).

Furthermore, the evaluation of microglia using the proliferative marker Ki67 in the hippocampus revealed minimal and similar proliferation rates in both AD-Veh and AD-EVs groups (AD-Veh group, Mean \pm SEM = $1.1 \pm 0.5\%$; AD-EVs group, $0.7 \pm 0.4\%$, $p > 0.05$, Figure S14). Additionally, analysis of IBA-1+ cells lacking TMEM119 expression revealed infiltrating macrophages among microglia (cells positive for both IBA-1 and TMEM119) in the hippocampus (Figure S15(A-F)). Lower percentages of infiltrating macrophages were observed in the female AD-EVs group compared to their counterparts in the AD-Veh group (Figure S15(H)). However, in male AD mice, percentages of infiltrating macrophages were comparable between Veh and EVs groups (Figure S15(G)). Two-way ANOVA analysis revealed no sex-dependent differences. However, there was an interaction between sex and EVs treatment, as only females showed positive response (Table S2).

3.6 | hiPSC-NSC-EVs treatment reduced astrocyte hypertrophy in the hippocampus of AD mice

Examples of the distribution and morphology of astrocytes in the CA3 subfield of the hippocampus from different groups are illustrated (Figure S16(A-C)). Compared to the naïve group, the AD-Veh group displayed increased GFAP+ astrocytic elements (Figure S16(D-K)) in subregions and the entire hippocampus in both male and female mice, implying the occurrence of astrocyte hypertrophy. The male AD-EVs group displayed significantly reduced astrocyte hypertrophy than the AD-Veh group in DG and CA3 regions and when the entire hippocampus was considered together ($p < 0.05$ – 0.001 , Figure S16(D, F-G)). Similar results were seen in female AD mice receiving EVs when the hippocampus was considered in entirety ($p < 0.05$, Figure S16(K)). Two-way ANOVA analysis revealed no sex-dependent differences or interactions between sex and EVs treatment.

3.7 | hiPSC-NSC-EVs treatment maintained lower expression of DAM genes for extended periods

We quantified and compared the expression of multiple DAM genes in the hippocampus at 5 months of age (i.e., ~2 months post-EV treatment) across groups. Compared to the naïve control group, the AD-Veh group displayed increased expression of *cst7*, *spp1*, *lpl*, *apoe*, *fth1*, and *tyrobp* in males ($p < 0.05$ – 0.0001 , Figure 6(a-f)) and *cst7*, *lpl*, *fth1*, *tyrobp*, and *ctsd* in females ($p < 0.05$ – 0.001 , Figure 6(i, k, m-n, p)). However, the expression of most of these genes in both males and females in the AD-EVs group was normalized to levels in the naïve group ($p > 0.05$, Figure 6(b-f, i, k, m, n, p)). The expression of some genes was also reduced in the AD-EVs group compared to the AD-Veh group ($p < 0.05$, Figure 6(a, c, d, i)). Thus, the modulatory effects of hiPSC-NSC-EVs treatment on DAM genes observed at 72 h post-EV administration persisted at ~2 months post-EV treatment, which could be gleaned from the similar expression pattern of multiple genes between naïve and AD-EVs groups. However, the extent of suppression was moderate compared to the AD-Veh group, as the expression of only a few genes significantly differed between the AD-Veh and AD-EVs groups. Furthermore, two-way ANOVA analysis revealed no sex-dependent effects or interactions between sex and hiPSC-NSC-EVs treatment for most genes linked to DAM in 5xFAD mice. The exception was *cst7*, with males showing a greater expression in both Veh and EVs groups. There was also an interaction between sex and EVs treatment for *cst7*, as only males showed positive responses (Table S2).

3.8 | hiPSC-NSC-EVs administration induced enduring inhibition of NLRP3 inflammasome activation

We first measured and compared the expression of genes linked to NLRP3 inflammasome activation across groups. The AD-Veh group displayed increased expression of *nlrp3*, *pycard/asc*, *il1b*, and *il18* genes in males ($p < 0.05$ – 0.01 ; Figure 6(q-r, t-u)) and

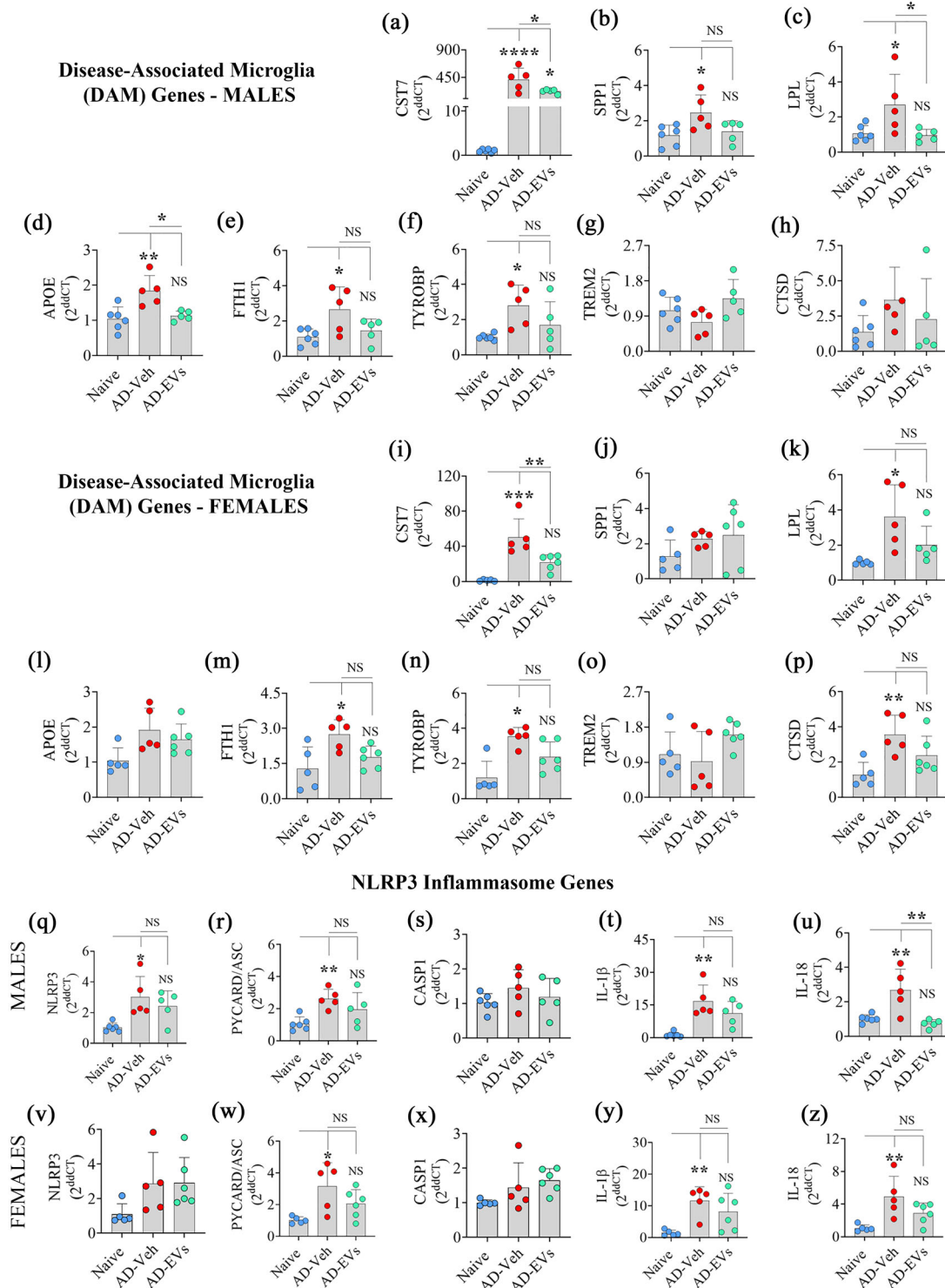


FIGURE 6 Intranasal administration of extracellular vesicles from human induced pluripotent stem cell-derived neural stem cells (hiPSC-NSC-EVs) to 5xFAD mice normalized the expression of genes linked to disease associated microglia (DAM) and inflammasome activation. The bar charts A-P compare the expression of DAM genes (*cst7*, *spp1*, *lpl*, *apoE*, *fth1*, *tyrobp*, *trem2*, *ctsd*) in the hippocampus of males (A-H) and females (I-P) between naïve, AD-Veh and AD-EVs groups. The bar charts Q-Z compare the expression of genes linked to NOD-, LRR- and pyrin domain-containing protein 3 (NLRP3) inflammasome activation (*nlrp3*, *pycard*, *caspl*, *il-1 β* , *il-18*) in hippocampus of males (Q-U) and females (V-Z) between naïve, AD-Veh and AD-EVs groups. *, $p < 0.05$; **, $p < 0.01$; ***, $p < 0.001$; ****, $p < 0.0001$; NS, not significant.

pycard/asc, *il1b*, and *il18* genes in females ($p < 0.05$ – 0.01 ; Figure 6(w,y,z). However, in the AD-EVs group, the expressions of these genes were normalized to levels in the naïve group ($p > 0.05$, Figure 6(q-r, t-u, w, y, z). Two-way ANOVA analysis revealed no sex-dependent differences or interactions between sex and hiPSC-NSC-EVs treatment for most genes linked to NLRP3 inflammasome activation in 5xFAD mice. The exceptions were *il18*, with females showing a greater expression in both Veh and EVs groups (Table S2). Next, we quantified the extent of NLRP3 inflammasome complexes within microglia in the hippocampus through triple immunofluorescence for IBA-1, NLRP3, and ASC. Examples of microglia displaying NLRP3 inflammasome complexes (i.e., structures co-expressing NLRP3 and ASC) are illustrated (Figure 7(a-i). Compared to the naïve group, both males and females in the AD-Veh group displayed increased percentages of microglia presenting inflammasome complexes ($p < 0.01$, Figure 7(j,k). On the other hand, percentages of microglia containing inflammasome complexes in both sexes of the AD-EVs group matched percentages in the naïve group ($p > 0.05$, Figure 7(j,k) and were less than their counterparts in the AD-EVs group ($p < 0.05$, Figure 7(j,k). To confirm these further, we quantified the concentrations of NLRP3 inflammasome activation mediators (NF κ B, NLRP3, ASC, and cleaved caspase-1) and end products (IL-1 β and IL-18) in the hippocampus. Compared to the naïve group, both sexes in the AD-Veh group displayed increased concentrations of all these proteins ($p < 0.05$ – 0.0001 , Figure 7(l-q, r-w). Notably, the concentrations of all these proteins were either normalized to levels in the naïve group ($p > 0.05$, Figure 7(m-o, q, r-w) or went below the level of the naïve group (Figure 7(l,p) in males and females in the AD-EVs group. Thus, the repressing effects of hiPSC-NSC-EVs on NLRP3 inflammasome genes observed at 72 h post-EV administration persisted at ~2 months post-EV treatment. Two-way ANOVA analysis showed sex-dependent differences for many proteins linked to NLRP3 inflammasome activation in 5xFAD mice. Males displayed higher concentrations of cleaved caspase-1 (AD-EVs group), IL-1 β (AD-Veh and AD-EVs groups), and IL-18 (AD-Veh group). Furthermore, the interaction between sex and hiPSC-NSC-EVs treatment was seen for NF- κ B and IL-1 β , with only males showing positive or higher responses (Table S2).

3.9 | hiPSC-NSC-EVs treatment prevented hyperactivation of p38/MAPK signalling

Increased release of proinflammatory cytokines IL-18 and IL-1 β following NLRP3 inflammasome activation leads to downstream p38/MAPK hyperactivation in acute and chronic inflammatory conditions (Kodali et al., 2023a). Therefore, we first compared the concentrations of different p38/MAPK signalling components, including MyD88, Ras, phospho-p38 MAPK, and AP-1 in naïve, AD-Veh, and AD-EVs groups. Next, we compared the concentrations of some known end products of p38/MAPK hyperactivation, including IL-6, TNF α , and IL-8 and Mip-1 α . Compared to the naïve group, males in the AD-Veh group displayed elevated levels of MyD88, Ras, p38/MAPK, and AP-1 levels ($p < 0.05$ – 0.01 ; Figure 8(a-d). Females in the AD-Veh group also showed a similar trend, but only Ras and p38/MAPK increases were statistically significant ($p < 0.05$ – 0.01 ; Figure 8(j,k). Notably, in the AD-EVs group, the concentrations of these proteins were normalized to levels in the naïve control group ($p > 0.05$, Figure 8(a-d, j, k). Furthermore, in both males and females, the concentrations of IL-8, TNF α , and Mip-1 α were elevated in the AD-Veh group but not in the AD-EVs group ($p < 0.05$ – 0.001 ; Figure 8(f-h, n-p). Females in the AD-Veh group, in addition, showed upregulation of IL-6 compared to the naïve group ($p < 0.01$; Figure 8(m)), which was normalized in the AD-EVs group ($p > 0.05$, Figure 8(m)). Thus, inhibition of NLRP3 inflammasome activation mediated by hNSC-EVs prevented the downstream hyperactivation of p38/MAPK signalling. Two-way ANOVA analysis showed sex-dependent differences for a few end products of p38/MAPK signalling activation in 5xFAD mice, with males in both Veh and EVs groups displaying higher concentrations of TNF α and MIP1 α . Furthermore, the interaction between sex and hiPSC-NSC-EVs treatment was seen for Ras, with only males showing positive or higher responses (Table S2).

3.10 | hiPSC-NSC-EVs administration induced enduring inhibition of cGAS-STING signalling

We quantified the concentrations of various proteins causing the activation of the cGAS-STING pathway, an upstream event activating IFN-1 signalling in AD and 5xFAD mice (Xie et al., 2023). Compared to the naïve group, the hippocampus from the AD-Veh group displayed increased concentrations of total cGAS, p-STING, p-IRF3, and IFN- α in males ($p < 0.05$ – 0.01 , Figure 8(q-t)), and p-STING and p-IRF3 in females ($p < 0.05$, Figure 8(v-w). In contrast, in the AD-EVs group, the concentrations of these proteins in both sexes did not differ from the naïve group ($p > 0.05$, Figure 8(q-x). Thus, the modulatory effects of hiPSC-NSC-EVs on IFN-1 signalling observed at 72 h post-EV administration persisted at ~2 months post-EV treatment. Two-way ANOVA analysis showed sex-dependent differences for IFN α levels in AD-Veh and AD-EVs groups. However, there was no interaction between sex and hiPSC-NSC-EVs treatment (Table S2). Furthermore, evaluation of dsDNA in the cytoplasm of microglia revealed significant amount of dsDNA accumulation in both males and females in the AD-Veh group (Figure S17(A-C). Notably, hiPSC-NSC-EVs treatment reduced the percentage of microglia containing dsDNA in male AD mice ($p < 0.01$) but not in female AD mice (Figure S17(G-H). Two-way ANOVA analysis revealed no sex-dependent differences or interaction between sex and EVs treatment.

IBA-1+ Microglia Expressing Activated NLRP3 Inflammasome in Hippocampus

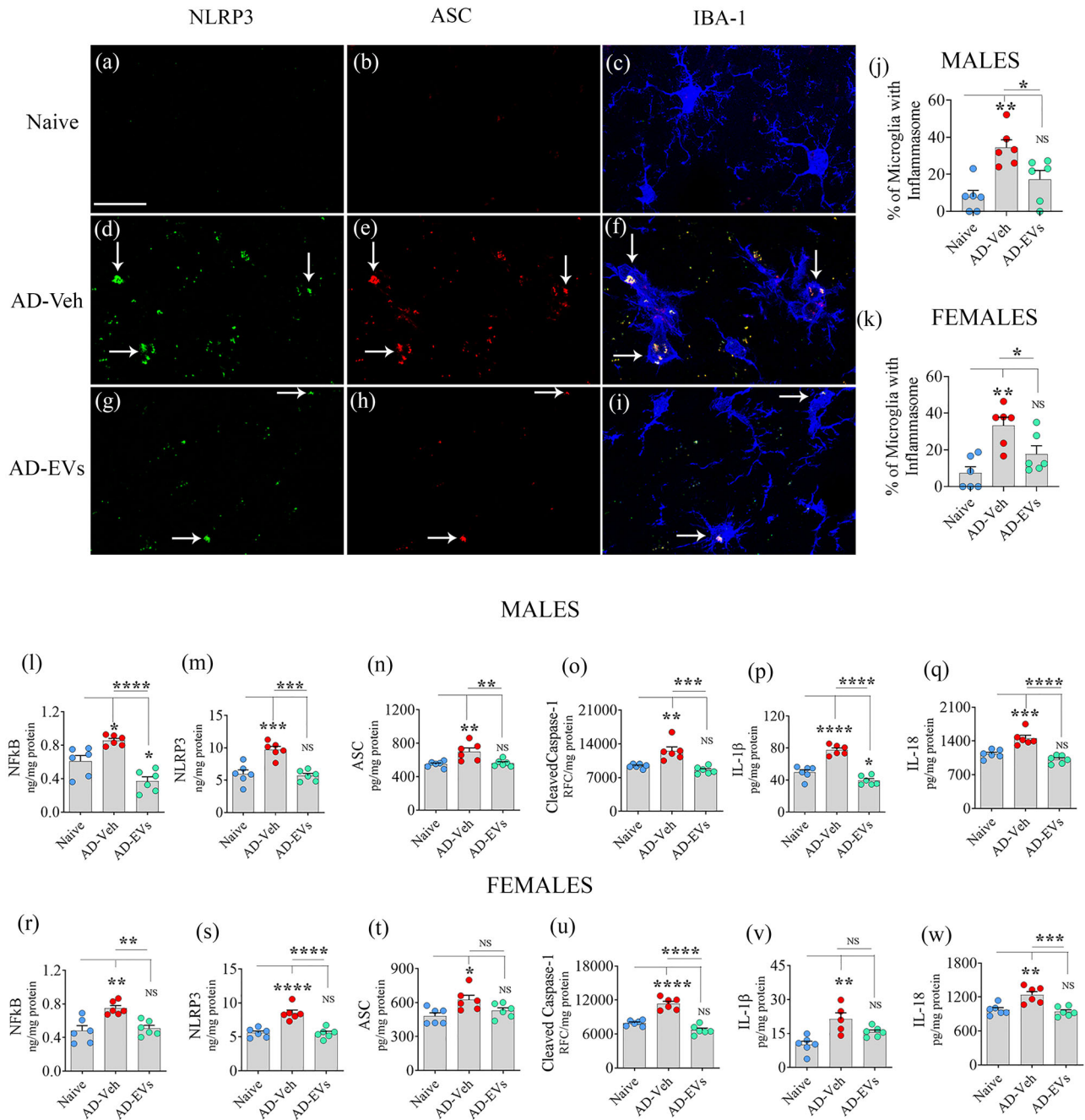


FIGURE 7 Intranasal administration of extracellular vesicles from human induced pluripotent stem cell-derived neural stem cells (hiPSC-NSC-EVs) to 5xFAD mice inhibited NOD-, LRR- and pyrin domain-containing protein 3 (NLRP3) inflammasome complex formation and activation. Figures (A-I) illustrate examples of NLRP3 inflammasome complexes co-expressing NLRP3 (green) and apoptosis-associated speck-like protein containing a CARD (ASC, red) in IBA-1+ microglia (blue) from the CA3 subfield of the hippocampus in male mice from naïve (A-C), AD-Veh (D-F), and AD-EVs (G-I) groups. The bar charts J-K compare the percentages of microglia with inflammasome complexes in males (J) and females (K). The bar charts L-W compare the concentrations of mediators of NLRP3 inflammasome activation (NF-κB, NLRP3, ASC, and cleaved caspase-1; L-O, males and R-U, females) and end products (IL-1β, IL-18; P-Q, and V-W) in males (L-Q) and females (R-W) between naïve, AD-Veh, and AD-EVs groups. Scale bar, A-I = 25 μm; *, $p < 0.05$; **, $p < 0.01$; ***, $p < 0.001$; ****, $p < 0.0001$; NS, not significant.

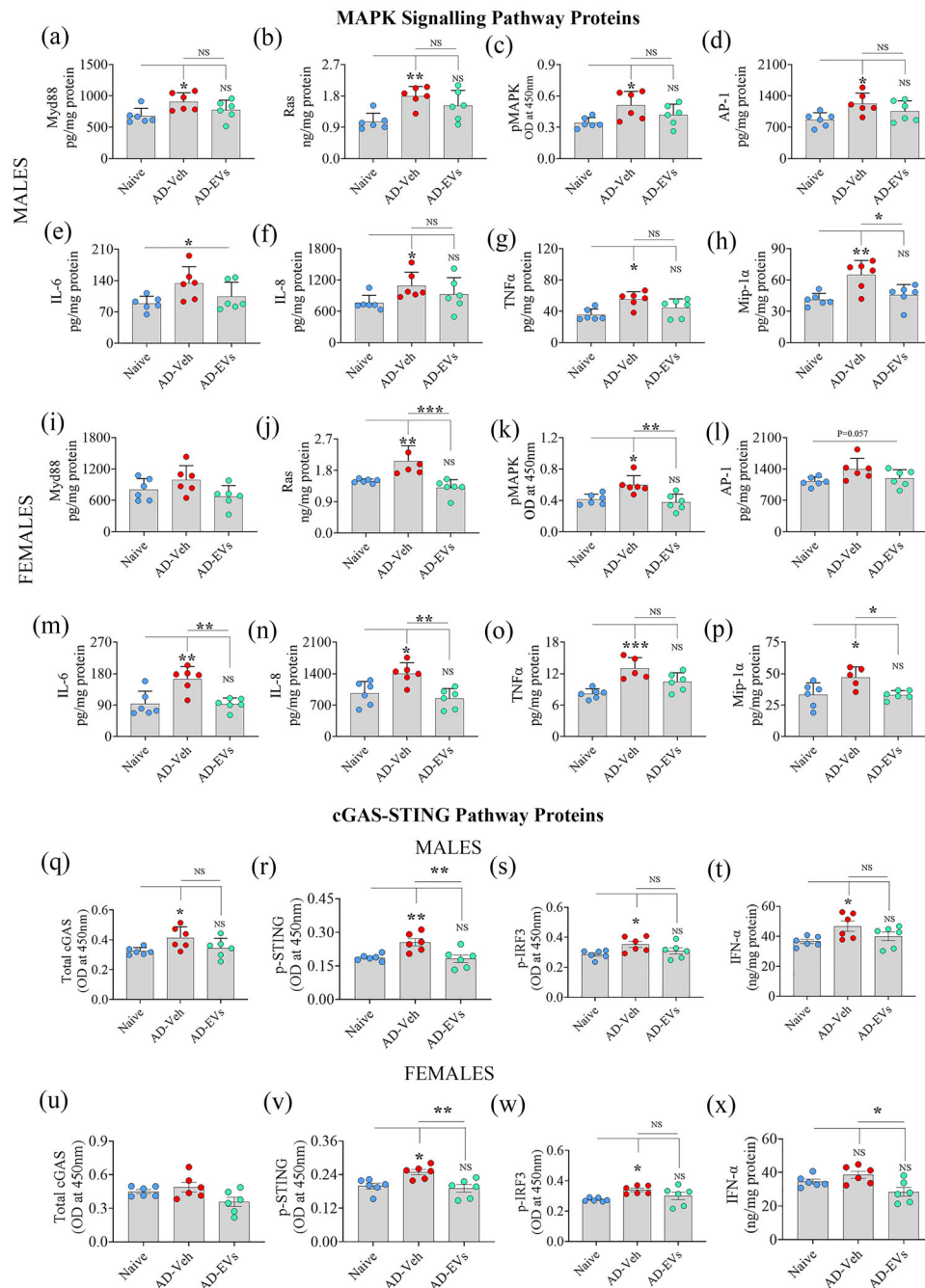


FIGURE 8 Intranasal administration of extracellular vesicles from human induced pluripotent stem cell-derived neural stem cells (hiPSC-NSC-EVs) to 5xFAD mice thwarted the activation of p38 mitogen-activated protein kinase and cyclic GMP-AMP synthase (cGAS), and phosphorylated stimulator of interferon genes (p-STING) signalling. The bar charts A-P compare the concentrations of various components of p38/MAPK activation (MyD88, Ras, pMAPK, AP-1; A-D and I-L) and end products (IL-6, IL-8, TNF α , Mip-1 α ; E-H and M-P) in males (a-h) and females (i-p) between naive, AD-Veh, and AD-EVs groups. *, $p < 0.05$; **, $p < 0.01$; ***, $p < 0.001$; NS, not significant. The bar charts Q-X compare total cyclic GMP-AMP synthase (cGAS, q, u), stimulator of interferon genes (p-STING, r, v), p-interferon regulatory factor 3 (p-IRF3, s, w), IFN- α (t, x) across groups in males (q-t) and females (u-x). *, $p < 0.05$; **, $p < 0.01$; ***, $p < 0.001$; NS, not significant.

3.11 | hiPSC-NSC-EVs administration reduced amyloid plaque load and p-tau

Comparing area fractions of brain tissue covered by amyloid plaques in the hippocampus revealed that males and females in the AD-EVs group displayed significantly lower plaque load than the AD-Veh group ($p < 0.05$, Figure 9(a-d)). Also, the hippocampal concentrations of soluble A β 42 were reduced in males and females of the AD-EVs group compared to the AD-Veh group ($p < 0.05-0.01$; Figure 9(e-f)). Furthermore, the hippocampal concentrations of p-tau were reduced in males and females

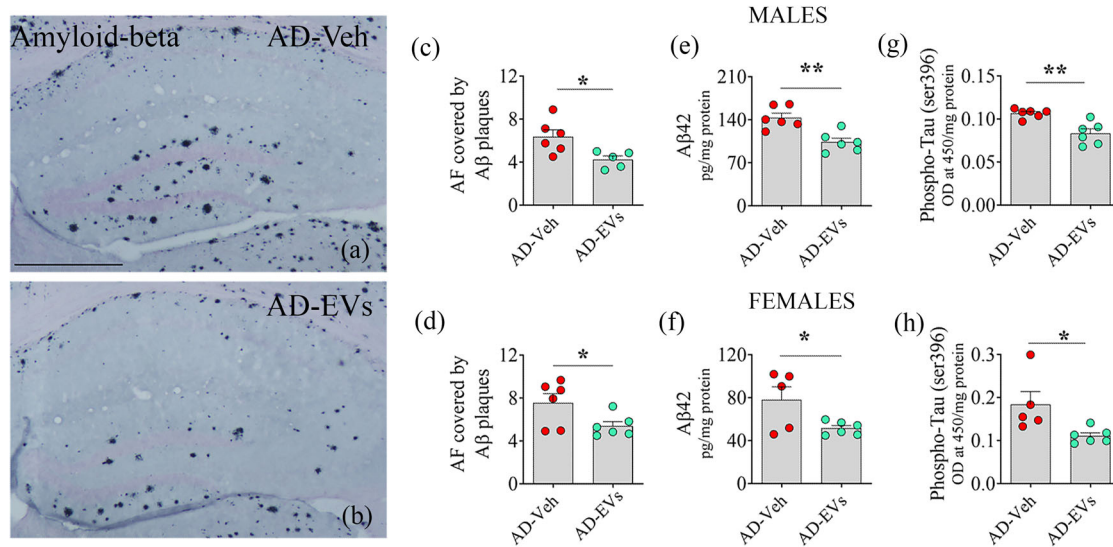


FIGURE 9 Intranasal administration of extracellular vesicles from human induced pluripotent stem cell-derived neural stem cells (hiPSC-NSC-EVs) to 5xFAD mice reduced amyloid plaques and phosphorylated tau. Figures (A–B) illustrate the distribution of amyloid plaques in the hippocampus from 5xFAD mice receiving the vehicle (Veh, A) or hiPSC-NSC-EVs (B). The bar charts compare area fraction (AF) of amyloid plaques (C, D), the concentration of soluble Aβ42 (E, F), and p-tau (G, H) in males (C, E, G) and females (D, F, H) between AD-Veh and AD-EVs groups. Scale bar, A–B = 500 μm; *, $p < 0.05$; **, $p < 0.01$; NS, not significant.

of the AD-EVs group compared to the AD-Veh group ($p < 0.05–0.01$; Figure 9(g–h)). Thus, hiPSC-NSC-EV-mediated reductions in neuroinflammatory cascades led to reduced amyloid plaques, Aβ42 production, and p-tau in the 5xFAD mouse brain. Two-way ANOVA analysis showed sex-dependent differences for the concentrations of Aβ–42 and p-tau, with higher Aβ–42 levels in males in AD-Veh and AD-EVs groups and greater p-tau levels in females in the AD-Veh group. There was also interaction between sex and hiPSC-NSC-EVs treatment for Aβ–42, as males showed greater responses (Table S2).

3.12 | hiPSC-NSC-EVs administration did not impact the phagocytotic activity of microglia

Animals receiving m-X04 were evaluated for in vivo labelling of Aβ42 plaques and particles in both AD-Veh and AD-EVs groups. The percentages of microglia phagocytosing m-X04 bound Aβ42 around and between plaques were comparable between the AD-Veh and AD-EVs groups ($p > 0.05$, Figure S18). Thus, hiPSC-NSC-EV treatment did not reduce the phagocytotic activity of microglia despite significantly modulating their gene expression.

4 | DISCUSSION

The results of this study, in male and female 5xFAD mouse models, provide evidence for the first time that IN administrations of hiPSC-NSC-EVs in the early stage of AD could restrain neuroinflammatory signalling cascades, and the extent of Aβ plaques and p-tau in the hippocampus and thereby maintain better cognitive and mood function at an advanced stage of the disease. While earlier studies have documented the effects of mouse NSC-EVs, mouse induced-NSC-EVs, and human embryonic stem cell-derived NSC-EVs to alleviate cognitive dysfunction, Aβ plaques, and neuroinflammation in general (Apodaca et al., 2021; Giannoni et al., 2016), the ability of hNSC-EVs to inhibit chronic neuroinflammatory signalling cascades by directly inducing transcriptomic changes in microglia and astrocytes has not been investigated.

In this study, 5xFAD mice received hiPSC-NSC-EVs at 3 months of age, an age at which these mice start to display Aβ plaques, microgliosis, and a proinflammatory milieu in the brain (Boza-Serrano et al., 2018; Gao et al., 2023), and interrogated with behavioural tests at ~4.5 months of age, a stage where untreated 5xFAD mice display cognitive and mood impairments (Oakley et al., 2006; Tang et al., 2016). The neuropathology was assessed at 5 months of age, a timepoint in which 5xFAD mice exhibited increased microglial activation with upregulation of multiple DAM genes, and activation of NLRP3 inflammasomes, and the p38/MAPK and cGAS-STING-IFN-1 signalling cascades. Remarkably, male, and female 5xFAD mice receiving hiPSC-NSC-EVs displayed better cognitive function and no anhedonia at 4.5 months of age compared to their counterparts receiving the vehicle. Moreover, hiPSC-NSC-EVs treatment led to reductions in the expression of genes and/or proteins linked to DAM, NLRP3,

p38/MAPK, and cGAS-STING-IFN-1 hyperactivation without compromising the phagocytosis function of microglia at 5 months of age. A β plaques, A β 42, and p-tau concentrations were also reduced.

The concept of using hiPSC-NSC-EVs to restrain the neuroinflammatory cascades involved in AD pathogenesis stemmed from our earlier studies demonstrating the proficiency of these EVs to mediate robust anti-inflammatory properties. For example, hiPSC-NSC-EVs have shown proficiency to suppress IL-6 release from lipopolysaccharide (LPS)-stimulated mouse macrophages, and IL-1 β and TNF α release from LPS-stimulated human iMicroglia (Upadhyaya et al., 2020, 2022). They also thwarted neuroinflammation after a brain insult such as status epilepticus (Upadhyaya et al., 2020) or LPS-induced peripheral inflammation (Ayyubova et al., 2023). Furthermore, these EVs are inherently enriched with anti-inflammatory miRNAs and proteins, evidenced by small RNA sequencing and proteomic studies (Upadhyaya et al., 2020). Our previous protein knockdown and miRNA inhibition studies have identified miR-21-5p and pentraxin-3 (PTX3) as the key anti-inflammatory molecules in these EVs (Upadhyaya et al., 2022). Such findings are consistent with the ability of miR-21-5p to regulate NF- κ B, enhance IL-10, and inhibit TNF α release (Ge et al., 2016; Sheedy, 2015; Slota & Booth, 2019) and the proficiency of PTX3 to enhance the neuroprotective type 2 astrocytes, and regulate the entry of peripheral immune cells into the brain (Rajkovic et al., 2019; Shindo et al., 2016). hiPSC-NSC-EVs also carry miR-103a, proficient in reducing neuroinflammation via prostaglandin-endoperoxide synthase-2 inhibition (Yang et al., 2018), hemopexin capable of transforming proinflammatory microglia into anti-inflammatory phenotypes (Han et al., 2018), and galectin-3 binding protein (Gal-3BP) competent in diminishing the NF- κ B signalling (Seki et al., 2020).

The entry of hiPSC-NSC-EVs into microglia in all brain regions led to reduced expression of multiple genes linked to DAM, NLRP3 inflammasome activation, and IFN-1 signalling. Such changes implying the modulation of activated microglia have implications because microglia, though recognize and remove a significant amount of A β in the early stage of AD, undergo hyperactivation, perpetuate chronic neuroinflammation, and contribute to disease progression and dementia in the advanced stage (Heneka et al., 2015; Mosher & Wyss-Coray, 2014; Perry & Holmes, 2014). Such transformed microglia lose homeostatic molecules and functions (Holtman et al., 2015) and acquire DAM or “neurodegenerative” phenotype (Friedman et al., 2018). DAM is typified by downregulation of “homeostatic” microglial genes *p2ry12*, *p2ry13*, *cx3cr1*, *cd33*, and *tmem119* (Butovsky et al., 2014) and upregulation of genes involved in lysosomal, phagocytic, and lipid metabolism pathways such as *apoe*, *ctsd*, *lpl*, *tyrobp*, and *trem2* (Deczkowska et al., 2018; Lambert et al., 2013). Notably, hiPSC-NSC-EVs-mediated transformation of microglia involved increased expression of homeostatic genes and reduced expression of DAM genes, implying the proficiency of hiPSC-NSC-EVs to transform DAM into less inflammatory microglia. Notably, such transformation did not impact phagocytosis activity of microglia. Testing the effects of hiPSC-NSC-EVs on human iMicroglia exposed to A β oligomers also confirmed the competence of hiPSC-NSC-EVs to downregulate DAM gene expression in activated human iMicroglia. Administration of hiPSC-NSC-EVs also modulated astrocytes, which could be gleaned from reduced expression of multiple genes linked to IFN-1 and IL-6 signalling. Since hiPSC-NSC-EVs were rarely internalized by astrocytes but consistently encounter the plasma membranes of their soma and processes (Attaluri et al., 2023), modulation of astrocytes likely involved the transfer of EV cargo through the fusion of EV membranes with the plasma membranes of astrocytes. However, an indirect effect of the modulation of microglia on astrocytes cannot be ruled out, either. Additional studies using engineered hiPSC-NSC-EVs capable of targeting only microglia are needed to address this issue.

hiPSC-NSC-EVs treatment normalized/reduced the expression of many genes linked to the NLRP3 inflammasome activation. Similar effects were also seen in human iMicroglia exposed to A β oligomers. Activation of NLRP3 inflammasomes within microglia in AD occurs as a response to A β , as A β fibrils can induce IL-1 β release from glia through NLRP3 inflammasome activation, and A β oligomers and fibrils can directly interact with NLRP3 inflammasome components and induce its activation (Akama & Van Eldik, 2000; Halle et al., 2008; Nakanishi et al., 2018). Additionally, p-tau-derived paired helical filament-6 (PHF6) peptides can induce NLRP3 inflammasome activation (Panda et al., 2021). Inhibition of NLRP3 inflammasome activation is beneficial because of its contribution to AD pathogenesis, particularly its ability to perpetuate chronic neuroinflammation via downstream hyperactivation of p38/MAPK signalling, increase tau phosphorylation, and induce cognitive dysfunction. Such concept is supported by findings of increased NLRP3 inflammasome end products (IL-1 β and IL-18) in AD patients (Ojala et al., 2009; Torres et al., 2014), and better cognitive function, reduced chronic neuroinflammation and A β 42 in AD models with the inhibition of NLRP3 inflammasome activation (Dempsey et al., 2017; Heneka et al., 2013; Lonnemann et al., 2020). A β induced tau pathology is also linked to NLRP3 inflammasome activation, as NLRP3 knockout in tauopathy mice reduced tau phosphorylation by regulating tau kinases and phosphatases (Ising et al., 2019).

IN administration of hiPSC-NSC-EVs also normalized/reduced the expression of many genes linked to IFN-1, IFN- γ , and IL-6 signalling within microglia, and IFN-1 and IL-6 signalling within astrocytes, in 5xFAD mice. Type-I IFNs, including IFN- α and IFN- β , bind to the IFN-1 receptor complex and activate signalling via kinases JAK1 and tyrosine kinase 2, leading to STAT1 and STAT2 phosphorylation, which results in the upregulation of thousands of interferon-stimulated genes (ISGs) (Shaw et al., 2017). Type-I IFNs are chronically activated within dysfunctional microglia in AD (Navarro et al., 2018), and IFN α / β transcripts and ISGs are upregulated in the brains of AD patients (Roy et al., 2020; Taylor et al., 2014). Also, the expression of IRF7, a transcription factor controlling IFN-1 signalling correlates with AD progression (Roy et al., 2020; Taylor et al., 2014). Furthermore, both amyloid and tau models of AD display an increased population of IFN-responsive microglia overexpressing ISGs (Rexach

et al., 2020; Yang et al., 2021). While type-I IFNs protect against infection, their overproduction in neurodegenerative conditions can cause adverse effects, including increased synapse loss, microglial activation, and aggregation of A β 42 and p-tau (Minter et al., 2016, 2022; Roy et al., 2020). On the other hand, increased IFN- γ signalling in microglia can transform them into neurotoxic phenotypes capable of impairing neural network rhythms and cognitive functions, and causing neurodegeneration (Kann et al., 2022). Additionally, increased IL-6 can contribute to memory impairment in AD (Lyra et al., 2021). Thus, the adeptness of hiPSC-NSC-EVs to reduce IFN-1, IFN- γ , and IL-6 signalling within activated microglia in 5xFAD mice is advantageous for slowing AD progression.

Furthermore, transcriptomic changes induced by hiPSC-NSC-EVs on microglia and astrocytes in 5xFAD mice at 72 h post-EV administration persisted at 2 months post-EV treatment in the hippocampus. This was evidenced by male and female 5xFAD mice receiving hiPSC-NSC-EVs displaying reductions in (1) microglial clusters, (2) the expression of multiple genes linked to DAM and NLRP3 inflammasome activation, (3) percentages of microglia presenting NLRP3 inflammasomes, (4) the concentrations of NLRP3 inflammasome activation mediators and end products, (5) proteins involved in p38/MAPK hyperactivation, (6) multiple proinflammatory cytokines, and (7) astrocyte hypertrophy. Reduced clusters of microglia suggest reductions in PAM as such clusters are seen around A β plaques (Grubman et al., 2021), which is likely a consequence of diminished plaque density with hiPSC-NSC-EVs treatment. Reduced numbers of microglia found in male mice following EVs treatment did not appear to be due to reduced proliferation of microglia, as IBA-1+ cells expressing Ki67 were minimal and did not differ between AD-Veh and AD-EVs groups. Populations of infiltrating macrophages were seen in both AD-Veh and AD-EVs groups, with female AD mice showing reduced infiltrating macrophages following hiPSC-NSC-EVs treatment. Thus, reduced microglia following hiPSC-NSC-EVs treatment observed in the male AD mice is likely due to increased clearance of pathological microglia.

Reduced percentages of microglia displaying NLRP3 inflammasome complexes in male and female AD mice indicate reduced microglial activation (Liang et al., 2022). Such changes in microglia were associated with reductions in the expression of genes linked to DAM and NLRP3 inflammasomes and the concentration of proteins linked to NLRP3 inflammasome activation (NF- κ B, NLRP3, ASC, cleaved caspase-1 and IL-1 β and IL-18). Dampened NLRP3 inflammasome activation led to reduced secretion of IL-1 β and IL-18, which prevented the hyperactivation of p38/MAPK signalling. Such an effect was evidenced by reduced concentrations of MyD88, Ras, pMAPK, and AP-1, IL-6, IL-8, TNF α , and Mip-1 α . Preventing the hyperactivation of p38/MAPK signalling in AD is beneficial because p38/MAPK promotes NF- κ B activation, tau phosphorylation, and glutamate excitotoxicity, impairs synaptic plasticity and autophagy and promotes neurodegeneration (Kheiri et al., 2018). Moreover, knockdown of p38/MAPK has been shown to alleviate microglia activation and postpone cognitive decline in animal models of AD (Gee et al., 2020; Son et al., 2023). Additionally, at ~2 months post-EV treatment, animals in the AD-EVs group displayed diminished cGAS-STING activation implicated in IFN-1 signalling (Xie et al., 2023).

In both AD models and patients, A β plaques increase progressively and are surrounded by activated microglia with DAM genes signature and an impaired ability for phagocytosis and A β clearance (Hickman et al., 2008; Meyer-Luehmann et al., 2008). Although hiPSC-NSC-EVs treatment transformed microglia into less inflammatory states, evident from the reduced expression of DAM and NLRP3 inflammasome genes and diminished clustering (Deczkowska et al., 2018; Lambert et al., 2013), such transformation did not alter the overall proficiency of microglia for A β phagocytosis based on the *in vivo* m-X04 assay results in this study. Considering these, decreased formation of A β plaques following hiPSC-NSC-EVs treatment likely involved two mechanisms. First, since overly activated microglia spread A β seeds to form new plaques (Clayton et al., 2021; d'Errico et al., 2022), modulation of activated microglia by hiPSC-NSC-EVs likely diminished such seeding. Second, hiPSC-NSC-EVs are naturally enriched with Gal-3BP, which can suppress A β production by inhibiting β -secretase (Seki et al., 2020). Such an effect is supported by the reduced concentration of A β 42 in the hippocampus of the AD-EVs group. On the other hand, reduced p-tau in the AD-EVs group is a consequence of diminished NLRP3 inflammasome activation, as A β induced tau pathology is linked to the extent of NLRP3 inflammasome activation (Ising et al., 2019).

In conclusion, IN administrations of hiPSC-NSC-EVs in 5xFAD mice resulted in their interaction with microglia and astrocytes, which led to alterations in microglial and astrocytic transcriptomic signature and sustained reductions in downstream neuroinflammatory signalling cascades and better cognitive and mood function. Notably, the beneficial effects of hiPSC-NSC-EVs treatment on microglia, astrocytes, infiltrating macrophages, amyloid plaques, p-tau levels, and cognitive and mood function in 5xFAD mice were not sex-dependent, as no interactions were observed between sex and EVs treatment for these parameters. The exceptions include the concentrations of NF- κ B, IL-1 β , Ras, and soluble A β -42, for which only males exhibited significant declines, or males showed greater declines than females following EVs treatment. The results also imply that microglia- and astrocyte-mediated chronic neuroinflammation in AD contributes profoundly to the progression of cognitive and mood function decline, and EV-based biologics capable of modulating their overactivation without affecting their homeostatic and A β clearing functions can considerably slow down the progression of AD pathogenesis. However, since neurons also incorporate IN administered hiPSC-NSC-EVs in 5xFAD mice (Attaluri et al., 2023), it will be important in future studies to examine changes occurring in neurons and the contribution of hiPSC-NSC-EVs induced neuronal plasticity to improved cognitive and mood function.

AUTHOR CONTRIBUTIONS

Concept: Ashok K. Shetty. **Research design:** Ashok K. Shetty, Leelavathi N. Madhu, Maheedhar Kodali, Raghavendra Upadhy, Shama Rao, and James J. Cai. **Data collection, analysis, and interpretation:** Leelavathi N. Madhu, Maheedhar Kodali, Raghavendra Upadhy, Shama Rao, Yogish Somayaji, Sahithi Attaluri, Bing Shuai, Maha Kirmani, Shreyan Gupta, Nathaniel Maness, Xiaolan Rao, James J. Cai, and Ashok K. Shetty. **Preparation of figure composites:** Leelavathi N. Madhu, Maheedhar Kodali, Shama Rao, Yogish Somayaji, Sahithi Attaluri, and Ashok K. Shetty. **Manuscript writing:** Leelavathi N. Madhu and Ashok K. Shetty. All authors provided feedback, edits, and additions to the manuscript text and approved the final version of the manuscript.

ACKNOWLEDGEMENTS

The TEM images of hiPSC-NSC-EVs were taken at the Image Analysis Laboratory, Texas A&M Veterinary Medicine & Biomedical Sciences (RRIS: SCR_0222479). Supported by grants from the National Institute for Aging (1RFIAG074256-01 and R01AG075440-01 to A.K.S.).

CONFLICT OF INTEREST STATEMENT

The authors report no conflicts of interest.

DATA AVAILABILITY STATEMENT

Source data are included with this original research article. Any additional data requests are available from the corresponding author upon request.

ORCID

Ashok K. Shetty  <https://orcid.org/0000-0001-5049-6671>

REFERENCES

- Abdi, S., Javanmehr, N., Ghasemi-Kasman, M., Bali, H. Y., & Pirzadeh, M. (2022). Stem cell-based therapeutic and diagnostic approaches in Alzheimer's disease. *Current Neuropharmacology*, 20, 1093–1115. <https://doi.org/10.2174/1570159x20666211231090659>
- Akama, K. T., & Van Eldik, L. J. (2000). Beta-amyloid stimulation of inducible nitric-oxide synthase in astrocytes is interleukin-1beta- and tumor necrosis factor-alpha (TNFalpha)-dependent, and involves a TNFalpha receptor-associated factor- and NFkappaB-inducing kinase-dependent signalling mechanism. *Journal of Biological Chemistry*, 275, 7918–7924. <https://doi.org/10.1074/jbc.275.11.7918>
- Apodaca, L. A., Baddour, A. A. D., Garcia, C., Jr., Alikhani, L., Giedzinski, E., Ru, N., Agrawal, A., Acharya, M. M., & Baulch, J. E. (2021). Human neural stem cell-derived extracellular vesicles mitigate hallmarks of Alzheimer's disease. *Alzheimers Research & Therapy*, 13, 57. <https://doi.org/10.1186/s13195-021-00791-x>
- Attaluri, S., Jaimes Gonzalez, J., Kirmani, M., Vogel, A. D., Upadhy, R., Kodali, M., Madhu, L. N., Rao, S., Shuai, B., Babu, R. S., Huard, C., & Shetty, A. K. (2023). Intranasally administered extracellular vesicles from human induced pluripotent stem cell-derived neural stem cells quickly incorporate into neurons and microglia in 5xFAD mice. *Frontiers in Aging Neuroscience*, 15, 1200445. <https://doi.org/10.3389/fnagi.2023.1200445>
- Attwood, S. W., & Edell, M. J. (2019). iPSC-Cell Technology and the problem of genetic instability-can it ever be safe for clinical use? *Journal of Clinical Medicine*, 8, 288. <https://doi.org/10.3390/jcm8030288>
- Ayyubova, G., Kodali, M., Upadhy, R., Madhu, L. N., Attaluri, S., Somayaji, Y., Shuai, B., Rao, S., Shankar, G., & Shetty, A. K. (2023). Extracellular vesicles from hiPSC-NSCs can prevent peripheral inflammation-induced cognitive dysfunction with inflammasome inhibition and improved neurogenesis in the hippocampus. *Journal of Neuroinflammation*, 20, 297. <https://doi.org/10.1186/s12974-023-02971-y>
- Boza-Serrano, A., Yang, Y., Paulus, A., & Deierborg, T. (2018). Innate immune alterations are elicited in microglial cells before plaque deposition in the Alzheimer's disease mouse model 5xFAD. *Scientific Reports*, 8, 1550. <https://doi.org/10.1038/s41598-018-19699-y>
- Butovsky, O., Jedrychowski, M. P., Moore, C. S., Cialic, R., Lanser, A. J., Gabriely, G., Koeglsperger, T., Dake, B., Wu, P. M., Doykan, C. E., Fanek, Z., Liu, L., Chen, Z., Rothstein, J. D., Ransohoff, R. M., Gygi, S. P., Antel, J. P., & Weiner, H. L. (2014). Identification of a unique TGF-beta-dependent molecular and functional signature in microglia. *Nature Neuroscience*, 17, 131–143. <https://doi.org/10.1038/nn.3599>
- Cai, J. J. (2020). scGEAToolbox: a Matlab toolbox for single-cell RNA sequencing data analysis. *Bioinformatics*, 36, btz830. <https://doi.org/10.1093/bioinformatics/btz830>
- Clayton, K., Delpech, J. C., Herron, S., Iwahara, N., Ericsson, M., Saito, T., Saido, T. C., Ikezu, S., & Ikezu, T. (2021). Plaque associated microglia hyper-secrete extracellular vesicles and accelerate tau propagation in a humanized APP mouse model. *Molecular Neurodegeneration*, 16, 18. <https://doi.org/10.1186/s13024-021-00440-9>
- Contreras, M. P., Mendez, M., Shan, X., Fechner, J., Sawangjit, A., Born, J., & Inostroza, M. (2024). Context memory formed in medial prefrontal cortex during infancy enhances learning in adulthood. *Nature Communications*, 15, 2475. <https://doi.org/10.1038/s41467-024-46734-6>
- Cossetti, C., Iraci, N., Mercer, T. R., Leonardi, T., Alpi, E., Drago, D., Alfaro-Cervello, C., Saini, H. K., Davis, M. P., Schaeffer, J., Vega, B., Stefanini, M., Zhao, C., Muller, W., Garcia-Verdugo, J. M., Mathivanan, S., Bachi, A., Enright, A. J., Mattick, J. S., & Pluchino, S. (2014). Extracellular vesicles from neural stem cells transfer IFN-gamma via Ifngr1 to activate Stat1 signalling in target cells. *Molecular Cell*, 56, 193–204. <https://doi.org/10.1016/j.molcel.2014.08.020>
- Deczkowska, A., Keren-Shaul, H., Weiner, A., Colonna, M., Schwartz, M., & Amit, I. (2018). Disease-associated microglia: A universal immune sensor of neurodegeneration. *Cell*, 173, 1073–1081. <https://doi.org/10.1016/j.cell.2018.05.003>
- Dempsey, C., Rubio Araiz, A., Bryson, K. J., Finucane, O., Larkin, C., Mills, E. L., Robertson, A. A. B., Cooper, M. A., O'Neill, L. A. J., & Lynch, M. A. (2017). Inhibiting the NLRP3 inflammasome with MCC950 promotes non-phlogistic clearance of amyloid-beta and cognitive function in APP/PS1 mice. *Brain Behavior and Immunity*, 61, 306–316. <https://doi.org/10.1016/j.bbi.2016.12.014>
- Duyckaerts, C., Delatour, B., & Potier, M. C. (2009). Classification and basic pathology of Alzheimer disease. *Acta Neuropathologica*, 118, 5–36. <https://doi.org/10.1007/s00401-009-0532-1>
- Eckert, A., Huang, L., Gonzalez, R., Kim, H. S., Hamblin, M. H., & Lee, J. P. (2015). Bystander effect fuels human induced pluripotent stem cell-derived neural stem cells to quickly attenuate early stage neurological deficits after stroke. *Stem Cells Translational Medicine*, 4, 841–851. <https://doi.org/10.5966/sctm.2014-0184>

- d'Errico, P., Ziegler-Waldkirch, S., Aires, V., Hoffmann, P., Mezo, C., Erny, D., Monasor, L. S., Liebscher, S., Ravi, V. M., Joseph, K., Schnell, O., Kierdorf, K., Staszewski, O., Tahirovic, S., Prinz, M., & Meyer-Luehmann, M. (2022). Microglia contribute to the propagation of Abeta into unaffected brain tissue. *Nature Neuroscience*, 25, 20–25. <https://doi.org/10.1038/s41593-021-00951-0>
- Friedman, B. A., Srinivasan, K., Ayalon, G., Meilandt, W. J., Lin, H., Huntley, M. A., Cao, Y., Lee, S. H., Haddick, P. C. G., Ngu, H., Modrusan, Z., Larson, J. L., Kaminker, J. S., Brug van der, M. P., & Hansen, D. V. (2018). Diverse brain myeloid expression profiles reveal distinct microglial activation states and aspects of Alzheimer's disease not evident in mouse models. *Cell Reports*, 22, 832–847. <https://doi.org/10.1016/j.celrep.2017.12.066>
- Frost, G. R., & Li, Y. M. (2017). The role of astrocytes in amyloid production and Alzheimer's disease. *Open Biology*, 7, 170228. <https://doi.org/10.1098/rsob.170228>
- Gao, G., Li, C., Ma, Y., Liang, Z., Li, Y., Li, X., Fu, S., Wang, Y., Xia, X., & Zheng, J. C. (2023). Neural stem cell-derived extracellular vesicles mitigate Alzheimer's disease-like phenotypes in a preclinical mouse model. *Signal Transduction and Targeted Therapy*, 8, 228. <https://doi.org/10.1038/s41392-023-01436-1>
- Ge, X., Huang, S., Gao, H., Han, Z., Chen, F., Zhang, S., Wang, Z., Kang, C., Jiang, R., Yue, S., Lei, P., & Zhang, J. (2016). miR-21-5p alleviates leakage of injured brain microvascular endothelial barrier in vitro through suppressing inflammation and apoptosis. *Brain Research*, 1650, 31–40. <https://doi.org/10.1016/j.brainres.2016.07.015>
- Gee, M. S., Son, S. H., Jeon, S. H., Do, J., Kim, N., Ju, Y. J., Lee, S. J., Chung, E. K., Inn, K. S., Kim, N. J., & Lee, J. K. (2020). A selective p38alpha/beta MAPK inhibitor alleviates neuropathology and cognitive impairment, and modulates microglia function in 5XFAD mouse. *Alzheimers Research & Therapy*, 12, 45. <https://doi.org/10.1186/s13195-020-00617-2>
- Giannoni, P., Arango-Lievano, M., Neves, I. D., Rousset, M. C., Baranger, K., Rivera, S., Jeanneteau, F., Claeysen, S., & Marchi, N. (2016). Cerebrovascular pathology during the progression of experimental Alzheimer's disease. *Neurobiology of Disease*, 88, 107–117. <https://doi.org/10.1016/j.nbd.2016.01.001>
- Grubman, A., Choo, X. Y., Chew, G., Ouyang, J. F., Sun, G., Croft, N. P., Rossello, F. J., Simmons, R., Buckberry, S., Landin, D. V., Pflueger, J., Vandekolk, T. H., Abay, Z., Zhou, Y., Liu, X., Chen, J., Larcombe, M., Haynes, J. M., McLean, C., ... Polo, J. M. (2021). Transcriptional signature in microglia associated with Abeta plaque phagocytosis. *Nature Communications*, 12, 3015. <https://doi.org/10.1038/s41467-021-23111-1>
- Guttikonda, S. R., Sikkema, L., Tchieu, J., Saurat, N., Walsh, R. M., Harschnitz, O., Ciceri, G., Sneeboer, M., Mazutis, L., Setty, M., Zumbo, P., Betel, D., Witte de, L. D., Pe'er, D., & Studer, L. (2021). Fully defined human pluripotent stem cell-derived microglia and tri-culture system model C3 production in Alzheimer's disease. *Nature Neuroscience*, 24, 343–354. <https://doi.org/10.1038/s41593-020-00796-z>
- Halle, A., Hornung, V., Petzold, G. C., Stewart, C. R., Monks, B. G., Reinheckel, T., Fitzgerald, K. A., Latz, E., Moore, K. J., & Golenbock, D. T. (2008). The NALP3 inflammasome is involved in the innate immune response to amyloid-beta. *Nature Immunology*, 9, 857–865. <https://doi.org/10.1038/ni.1636>
- Han, D., Yu, Z., Liu, W., Yin, D., Pu, Y., Feng, J., Yuan, Y., Huang, A., Cao, L., & He, C. (2018). Plasma Hemopexin ameliorates murine spinal cord injury by switching microglia from the M1 state to the M2 state. *Cell Death & Disease*, 9, 181. <https://doi.org/10.1038/s41419-017-0236-8>
- Hattiangady, B., & Shetty, A. K. (2012). Neural stem cell grafting counteracts hippocampal injury-mediated impairments in mood, memory, and neurogenesis. *Stem Cells Translational Medicine*, 1, 696–708. <https://doi.org/10.5966/sctm.2012-0050>
- Heneka, M. T., Carson, M. J., El Khoury, J., Landreth, G. E., Brosseron, F., Feinstein, D. L., Jacobs, A. H., Wyss-Coray, T., Vitorica, J., Ransohoff, R. M., Herrup, K., Frautschi, S. A., Finsen, B., Brown, G. C., Verkhratsky, A., Yamanaka, K., Koistinaho, J., Latz, E., Halle, A., ... Kummer, M. P. (2015). Neuroinflammation in Alzheimer's disease. *Lancet Neurology*, 14, 388–405. [https://doi.org/10.1016/S1474-4422\(15\)70016-5](https://doi.org/10.1016/S1474-4422(15)70016-5)
- Heneka, M. T., Kummer, M. P., Stutz, A., Delekate, A., Schwartz, S., Vieira-Saecker, A., Griep, A., Axt, D., Remus, A., Tzeng, T. C., Gelpi, E., Halle, A., Korte, M., Latz, E., & Golenbock, D. T. (2013). NLRP3 is activated in Alzheimer's disease and contributes to pathology in APP/PS1 mice. *Nature*, 493, 674–678. <https://doi.org/10.1038/nature11729>
- Hering, C., & Shetty, A. K. (2023). Extracellular vesicles derived from neural stem cells, astrocytes, and microglia as therapeutics for easing TBI-induced brain dysfunction. *Stem Cells Translational Medicine*, 12, 140–153. <https://doi.org/10.1093/stcltm/szad004>
- Hickman, S. E., Allison, E. K., & El Khoury, J. (2008). Microglial dysfunction and defective beta-amyloid clearance pathways in aging Alzheimer's disease mice. *Journal of Neuroscience*, 28, 8354–8360. <https://doi.org/10.1523/JNEUROSCI.0616-08.2008>
- Holtman, I. R., Raj, D. D., Miller, J. A., Schaafsma, W., Yin, Z., Brouwer, N., Wes, P. D., Moller, T., Orre, M., Kamphuis, W., Hol, E. M., Boddeke, E. W., & Eggen, B. J. (2015). Induction of a common microglia gene expression signature by aging and neurodegenerative conditions: A co-expression meta-analysis. *Acta Neurologica Communications*, 3, 31. <https://doi.org/10.1186/s40478-015-0203-5>
- Huffels, C. F. M., Middeldorp, J., & Hol, E. M. (2023). Aβ pathology and neuron-glia interactions: A synaptocentric view. *Neurochemical Research*, 48, 1026–1046. <https://doi.org/10.1007/s11064-022-03699-6>
- Iraci, N., Gaude, E., Leonardi, T., Costa, A. S. H., Cossetti, C., Peruzzotti-Jametti, L., Bernstock, J. D., Saini, H. K., Gelati, M., Vescovi, A. L., Bastos, C., Faria, N., Occhipinti, L. G., Enright, A. J., Frezza, C., & Pluchino, S. (2017). Extracellular vesicles are independent metabolic units with asparaginase activity. *Nature Chemical Biology*, 13, 951–955. <https://doi.org/10.1038/nchembio.2422>
- Ising, C., Venegas, C., Zhang, S., Scheiblich, H., Schmidt, S. V., Vieira-Saecker, A., Schwartz, S., Albasset, S., McManus, R. M., Tejera, D., Griep, A., Santarelli, F., Brosseron, F., Opitz, S., Stunden, J., Merten, M., Kaye, R., Golenbock, D. T., Blum, D., ... Heneka, M. T. (2019). NLRP3 inflammasome activation drives tau pathology. *Nature*, 575, 669–673. <https://doi.org/10.1038/s41586-019-1769-z>
- Jain, S., Yoon, S. Y., Zhu, L., Brodbeck, J., Dai, J., Walker, D., & Huang, Y. (2012). Arf4 determines dentate gyrus-mediated pattern separation by regulating dendritic spine development. *PLoS ONE*, 7, e46340. <https://doi.org/10.1371/journal.pone.0046340>
- Jurga, A. M., Paleczna, M., & Kuter, K. Z. (2020). Overview of general and discriminating markers of differential microglia phenotypes. *Frontiers in Cellular Neuroscience*, 14, 198. <https://doi.org/10.3389/fncel.2020.00198>
- Kann, O., Almouhanna, F., & Chausse, B. (2022). Interferon gamma: A master cytokine in microglia-mediated neural network dysfunction and neurodegeneration. *Trends in Neuroscience*, 45, 913–927. <https://doi.org/10.1016/j.tins.2022.10.007>
- Kanno, T., Tsuchiya, A., & Nishizaki, T. (2014). Hyperphosphorylation of Tau at Ser396 occurs in the much earlier stage than appearance of learning and memory disorders in 5XFAD mice. *Behavioral Brain Research*, 274, 302–306. <https://doi.org/10.1016/j.bbr.2014.08.034>
- Kant van der, R., Goldstein, L. S. B., & Ossenkoppele, R. (2020). Amyloid-beta-independent regulators of tau pathology in Alzheimer disease. *Nature Reviews Neuroscience*, 21, 21–35. <https://doi.org/10.1038/s41583-019-0240-3>
- Kheiri, G., Dolatshahi, M., Rahmani, F., & Rezaei, N. (2018). Role of p38/MAPKs in Alzheimer's disease: Implications for amyloid beta toxicity targeted therapy. *Reviews in the Neurosciences*, 30, 9–30. <https://doi.org/10.1515/revneuro-2018-0008>
- Kodali, M., Madhu, L. N., Reger, R. L., Milutinovic, B., Upadhy, R., Attaluri, S., Shuai, B., Shankar, G., & Shetty, A. K. (2023b). A single intranasal dose of human mesenchymal stem cell-derived extracellular vesicles after traumatic brain injury eases neurogenesis decline, synapse loss, and BDNF-ERK-CREB signalling. *Frontiers in Molecular Neuroscience*, 16, 1185883. <https://doi.org/10.3389/fnmol.2023.1185883>
- Kodali, M., Madhu, L. N., Reger, R. L., Milutinovic, B., Upadhy, R., Gonzalez, J. J., Attaluri, S., Shuai, B., Gitai, D. L. G., Rao, S., Choi, J. M., Jung, S. Y., & Shetty, A. K. (2023a). Intranasally administered human MSC-derived extracellular vesicles inhibit NLRP3-p38/MAPK signalling after TBI and prevent chronic brain dysfunction. *Brain Behavior and Immunity*, 108, 118–134. <https://doi.org/10.1016/j.bbi.2022.11.014>

- Lambert, J. C., Ibrahim-Verbaas, C. A., Harold, D., Naj, A. C., Sims, R., Bellenguez, C., DeStafano, A. L., Bis, J. C., Beecham, G. W., Grenier-Boley, B., Russo, G., Thornton-Wells, T. A., Jones, N., Smith, A. V., Chouraki, V., Thomas, C., Ikram, M. A., Zelenika, D., Vardarajan, B. N., ... Amouyel, P. (2013). Meta-analysis of 74,046 individuals identifies 11 new susceptibility loci for Alzheimer's disease. *Nature Genetics*, *45*, 1452–1458. <https://doi.org/10.1038/ng.2802>
- Lau, S. F., Wu, W., Seo, H., Fu, A. K. Y., & Ip, N. Y. (2021). Quantitative in vivo assessment of amyloid-beta phagocytic capacity in an Alzheimer's disease mouse model. *STAR Protocols*, *2*, 100265. <https://doi.org/10.1016/j.xpro.2020.100265>
- Li, Q., Cao, Y., Dang, C., Han, B., Han, R., Ma, H., Hao, J., & Wang, L. (2020). Inhibition of double-strand DNA-sensing cGAS ameliorates brain injury after ischemic stroke. *EMBO Molecular Medicine*, *12*, e11002.
- Liang, T., Zhang, Y., Wu, S., Chen, Q., & Wang, L. (2022). The role of NLRP3 inflammasome in Alzheimer's disease and potential therapeutic targets. *Frontiers in Pharmacology*, *13*, 845185. <https://doi.org/10.3389/fphar.2022.845185>
- Long, J. M., & Holtzman, D. M. (2019). Alzheimer disease: An update on pathobiology and treatment strategies. *Cell*, *179*, 312–339. <https://doi.org/10.1016/j.cell.2019.09.001>
- Long, Q., Upadhyay, D., Hattiangady, B., Kim, D. K., An, S. Y., Shuai, B., Prockop, D. J., & Shetty, A. K. (2017). Intranasal MSC-derived A1-exosomes ease inflammation, and prevent abnormal neurogenesis and memory dysfunction after status epilepticus. *Proceedings of the National Academy of Sciences U S A*, *114*, E3536–E3545. <https://doi.org/10.1073/pnas.1703920114>
- Lonnemann, N., Hosseini, S., Marchetti, C., Skouras, D. B., Stefanoni, D., D'Alessandro, A., Dinarello, C. A., & Korte, M. (2020). The NLRP3 inflammasome inhibitor OLT1177 rescues cognitive impairment in a mouse model of Alzheimer's disease. *Proceedings of the National Academy of Sciences U S A*, *117*, 32145–32154. <https://doi.org/10.1073/pnas.2009680117>
- Lu, M. H., Ji, W. L., Chen, H., Sun, Y. Y., Zhao, X. Y., Wang, F., Shi, Y., Hu, Y. N., Liu, B. X., Wu, J. W., Xu, D. E., Zheng, J. W., Liu, C. F., & Ma, Q. H. (2021). Intranasal transplantation of human neural stem cells ameliorates Alzheimer's disease-like pathology in a mouse model. *Frontiers in Aging Neuroscience*, *13*, 650103. <https://doi.org/10.3389/fnagi.2021.650103>
- Lyra, E. S. N. M., Goncalves, R. A., Pascoal, T. A., Lima-Filho, R. A. S., Resende, E. P. F., Vieira, E. L. M., Teixeira, A. L., de Souza, L. C., Peny, J. A., Fortuna, J. T. S., Furigo, I. C., Hashiguchi, D., Miya-Coreixas, V. S., Clarke, J. R., Abisambra, J. F., Longo, B. M., Donato, J., Jr, Fraser, P. E., Rosa-Neto, P., ... De Felice, F. G. (2021). Pro-inflammatory interleukin-6 signalling links cognitive impairments and peripheral metabolic alterations in Alzheimer's disease. *Translational Psychiatry*, *11*, 251. <https://doi.org/10.1038/s41398-021-01349-z>
- Madhu, L. N., Attaluri, S., Kodali, M., Shuai, B., Upadhyay, R., Gitai, D., & Shetty, A. K. (2019). Neuroinflammation in Gulf War Illness is linked with HMGB1 and complement activation, which can be discerned from brain-derived extracellular vesicles in the blood. *Brain Behavior and Immunity*, *81*, 430–443. <https://doi.org/10.1016/j.bbi.2019.06.040>
- Madhu, L. N., Kodali, M., Attaluri, S., Shuai, B., Melissari, L., Rao, X., & Shetty, A. K. (2021). Melatonin improves brain function in a model of chronic Gulf War Illness with modulation of oxidative stress, NLRP3 inflammasomes, and BDNF-ERK-CREB pathway in the hippocampus. *Redox Biology*, *43*, 101973. <https://doi.org/10.1016/j.redox.2021.101973>
- Martin, U. (2017). Genome stability of programmed stem cell products. *Advanced Drug Delivery Reviews*, *120*, 108–117. <https://doi.org/10.1016/j.addr.2017.09.004>
- Meyer-Luehmann, M., Spiess-Jones, T. L., Prada, C., Garcia-Alloza, M., Calignon de, A., Rozkalne, A., Koenigsnecht-Talboo, J., Holtzman, D. M., Bacskai, B. J., & Hyman, B. T. (2008). Rapid appearance and local toxicity of amyloid-beta plaques in a mouse model of Alzheimer's disease. *Nature*, *451*, 720–724. <https://doi.org/10.1038/nature06616>
- Minter, M. R., Moore, Z., Zhang, M., Brody, K. M., Jones, N. C., Shultz, S. R., Taylor, J. M., & Crack, P. J. (2016). Deletion of the type-1 interferon receptor in APPSWE/PS1DeltaE9 mice preserves cognitive function and alters glial phenotype. *Acta Neuropathologica Communications*, *4*, 72. <https://doi.org/10.1186/s40478-016-0341-4>
- Morton, M. C., Neckles, V. N., Seluzicki, C. M., Holmberg, J. C., & Feliciano, D. M. (2018). Neonatal subventricular zone neural stem cells release extracellular vesicles that act as a microglial morphogen. *Cell Reports*, *23*, 78–89. <https://doi.org/10.1016/j.celrep.2018.03.037>
- Mosher, K. I., & Wyss-Coray, T. (2014). Microglial dysfunction in brain aging and Alzheimer's disease. *Biochemical Pharmacology*, *88*, 594–604. <https://doi.org/10.1016/j.bcp.2014.01.008>
- Nakanishi, A., Kaneko, N., Takeda, H., Sawasaki, T., Morikawa, S., Zhou, W., Kurata, M., Yamamoto, T., Akbar, S. M. F., Zako, T., & Masumoto, J. (2018). Amyloid beta directly interacts with NLRP3 to initiate inflammasome activation: Identification of an intrinsic NLRP3 ligand in a cell-free system. *Inflammation and Regeneration*, *38*, 27. <https://doi.org/10.1186/s41232-018-0085-6>
- Navarro, V., Sanchez-Mejias, E., Jimenez, S., Munoz-Castro, C., Sanchez-Varo, R., Davila, J. C., Vizuete, M., Gutierrez, A., & Vitorica, J. (2018). Microglia in Alzheimer's disease: Activated, dysfunctional or degenerative. *Frontiers in Aging Neuroscience*, *10*, 140. <https://doi.org/10.3389/fnagi.2018.00140>
- Oakley, H., Cole, S. L., Logan, S., Maus, E., Shao, P., Craft, J., Guillozet-Bongaarts, A., Ohno, M., Disterhoft, J., Van Eldik, L., Berry, R., & Vassar, R. (2006). Intraneuronal beta-amyloid aggregates, neurodegeneration, and neuron loss in transgenic mice with five familial Alzheimer's disease mutations: Potential factors in amyloid plaque formation. *Journal of Neuroscience*, *26*, 10129–10140. <https://doi.org/10.1523/JNEUROSCI.1202-06.2006>
- Ojala, J., Alafuzoff, I., Herukka, S. K., van Groen, T., Tanila, H., & Pirttila, T. (2009). Expression of interleukin-18 is increased in the brains of Alzheimer's disease patients. *Neurobiology of Aging*, *30*, 198–209. <https://doi.org/10.1016/j.neurobiolaging.2007.06.006>
- Pan, X. D., Zhu, Y. G., Lin, N., Zhang, J., Ye, Q. Y., Huang, H. P., & Chen, X. C. (2011). Microglial phagocytosis induced by fibrillar β -amyloid is attenuated by oligomeric β -amyloid: Implications for Alzheimer's disease. *Molecular Neurodegeneration*, *6*, 45. <https://doi.org/10.1186/1750-1326-6-45>
- Panda, C., Voelz, C., Habib, P., Mevissen, C., Pufe, T., Beyer, C., Gupta, S., & Slowik, A. (2021). Aggregated Tau-PHF6 (VQIVYK) potentiates NLRP3 inflammasome expression and autophagy in human microglial cells. *Cells*, *10*, 1652. <https://doi.org/10.3390/cells10071652>
- Perry, V. H., & Holmes, C. (2014). Microglial priming in neurodegenerative disease. *Nature Reviews Neurology*, *10*, 217–224. <https://doi.org/10.1038/nrneurol.2014.38>
- Rajkovic, I., Wong, R., Lemarchand, E., Tinker, R., Allan, S. M., & Pinteaux, E. (2019). Pentraxin 3 regulates neutrophil infiltration to the brain during neuroinflammation. *AMRC Open Research*, *1*, 10.12688/amrcopenres.12875.1
- Rao, M. S., Hattiangady, B., & Shetty, A. K. (2008). Status epilepticus during old age is not associated with enhanced hippocampal neurogenesis. *Hippocampus*, *18*, 931–944. <https://doi.org/10.1002/hipo.20449>
- Rexach, J. E., Polioudakis, D., Yin, A., Swarup, V., Chang, T. S., Nguyen, T., Sarkar, A., Chen, L., Huang, J., Lin, L. C., Seeley, W., Trojanowski, J. Q., Malhotra, D., & Geschwind, D. H. (2020). Tau pathology drives dementia risk-associated gene networks toward chronic inflammatory states and immunosuppression. *Cell Reports*, *33*, 108398. <https://doi.org/10.1016/j.celrep.2020.108398>
- Roy, E. R., Chiu, G., Li, S., Propson, N. E., Kanchi, R., Wang, B., Coarfa, C., Zheng, H., & Cao, W. (2022). Concerted type I interferon signaling in microglia and neural cells promotes memory impairment associated with amyloid beta plaques. *Immunity*, *55*, 879–894. <https://doi.org/10.1016/j.immuni.2022.03.018>
- Roy, E. R., Wang, B., Wan, Y. W., Chiu, G., Cole, A., Yin, Z., Propson, N. E., Xu, Y., Jankowsky, J. L., Liu, Z., Lee, V. M., Trojanowski, J. Q., Ginsberg, S. D., Butovsky, O., Zheng, H., & Cao, W. (2020). Type I interferon response drives neuroinflammation and synapse loss in Alzheimer disease. *Journal of Clinical Investigation*, *130*, 1912–1930. <https://doi.org/10.1172/JCI133737>

- Seki, T., Kanagawa, M., Kobayashi, K., Kowa, H., Yahata, N., Maruyama, K., Iwata, N., Inoue, H., & Toda, T. (2020). Galectin 3-binding protein suppresses amyloid-beta production by modulating beta-cleavage of amyloid precursor protein. *Journal of Biological Chemistry*, 295, 3678–3691. <https://doi.org/10.1074/jbc.RA119.008703>
- Selkoe, D. J. (1989). Biochemistry of altered brain proteins in Alzheimer's disease. *Annual Review of Neuroscience*, 12, 463–490. <https://doi.org/10.1146/annurev.ne.12.030189.002335>
- Shaw, A. E., Hughes, J., Gu, Q., Behdenna, A., Singer, J. B., Dennis, T., Orton, R. J., Varela, M., Gifford, R. J., Wilson, S. J., & Palmarini, M. (2017). Fundamental properties of the mammalian innate immune system revealed by multispecies comparison of type I interferon responses. *PLoS Biology*, 15, e2004086. <https://doi.org/10.1371/journal.pbio.2004086>
- Sheedy, F. J. (2015). Turning 21: Induction of miR-21 as a key switch in the inflammatory response. *Frontiers in Immunology*, 6, 19. <https://doi.org/10.3389/fimmu.2015.00019>
- Shetty, A. K., Attaluri, S., Kodali, M., Shuai, B., Shetty, G. A., Upadhy, D., Hattiangady, B., Madhu, L. N., Upadhy, R., Bates, A., & Rao, X. (2020). Monosodium luminol reinstates redox homeostasis, improves cognition, mood and neurogenesis, and alleviates neuro- and systemic inflammation in a model of Gulf War Illness. *Redox Biology*, 28, 101389. <https://doi.org/10.1016/j.redox.2019.101389>
- Shetty, A. K., & Upadhy, D. (2016). GABA-ergic cell therapy for epilepsy: Advances, limitations and challenges. *Neuroscience & Biobehavioral Reviews*, 62, 35–47. <https://doi.org/10.1016/j.neubiorev.2015.12.014>
- Shindo, A., Maki, T., Mandeville, E. T., Liang, A. C., Egawa, N., Itoh, K., Itoh, N., Borlongan, M., Holder, J. C., Chuang, T. T., McNeish, J. D., Tomimoto, H., Lok, J., Lo, E. H., & Arai, K. (2016). Astrocyte-derived pentraxin 3 supports blood-brain barrier integrity under acute phase of stroke. *Stroke; A Journal of Cerebral Circulation*, 47, 1094–1100. <https://doi.org/10.1161/STROKEAHA.115.012133>
- Slota, J. A., & Booth, S. A. (2019). MicroRNAs in neuroinflammation: Implications in disease pathogenesis. *Biomarker Discovery and Therapeutic Applications. Noncoding RNA*, 5, 35. <https://doi.org/10.3390/ncrna5020035>
- Son, S. H., Lee, N. R., Gee, M. S., Song, C. W., Lee, S. J., Lee, S. K., Lee, Y., Kim, H. J., Lee, J. K., Inn, K. S., & Kim, N. J. (2023). Chemical knockdown of phosphorylated p38 mitogen-activated protein kinase (MAPK) as a novel approach for the treatment of Alzheimer's disease. *ACS Central Science*, 9, 417–426. <https://doi.org/10.1021/acscentsci.2c01369>
- Tang, X., Wu, D., Gu, L. H., Nie, B. B., Qi, X. Y., Wang, Y. J., Wu, F. F., Li, X. L., Bai, F., Chen, X. C., Xu, L., Ren, Q. G., & Zhang, Z. J. (2016). Spatial learning and memory impairments are associated with increased neuronal activity in 5XFAD mouse as measured by manganese-enhanced magnetic resonance imaging. *Oncotarget*, 7, 57556–57570. [10.18632/oncotarget.11353](https://doi.org/10.18632/oncotarget.11353)
- Taylor, J. M., Minter, M. R., Newman, A. G., Zhang, M., Adlard, P. A., & Crack, P. J. (2014). Type-1 interferon signalling mediates neuro-inflammatory events in models of Alzheimer's disease. *Neurobiology of Aging*, 35, 1012–1023. <https://doi.org/10.1016/j.neurobiolaging.2013.10.089>
- Temple, S. (2023). Advancing cell therapy for neurodegenerative diseases. *Cell Stem Cell*, 30, 512–529. <https://doi.org/10.1016/j.stem.2023.03.017>
- Torres, K. C., Lima, G. S., Fiamoncini, C. M., Rezende, V. B., Pereira, P. A., Bicalho, M. A., Moraes, E. N., & Romano-Silva, M. A. (2014). Increased frequency of cluster of differentiation 14 (CD14+) monocytes expressing interleukin 1 beta (IL-1beta) in Alzheimer's disease patients and intermediate levels in late-onset depression patients. *International Journal of Geriatric Psychiatry*, 29, 137–143. <https://doi.org/10.1002/gps.3973>
- Upadhy, D., Hattiangady, B., Castro, O. W., Shuai, B., Kodali, M., Attaluri, S., Bates, A., Dong, Y., Zhang, S. C., Prockop, D. J., & Shetty, A. K. (2019). Human induced pluripotent stem cell-derived MGE cell grafting after status epilepticus attenuates chronic epilepsy and comorbidities via synaptic integration. *Proceedings of the National Academy of Sciences U S A*, 116, 287–296. <https://doi.org/10.1073/pnas.1814185115>
- Upadhy, R., Madhu, L. N., Attaluri, S., Gitai, D. L. G., Pinson, M. R., Kodali, M., Shetty, G., Zanirati, G., Kumar, S., Shuai, B., Weintraub, S. T., & Shetty, A. K. (2020). Extracellular vesicles from human iPSC-derived neural stem cells: MiRNA and protein signatures, and anti-inflammatory and neurogenic properties. *Journal of Extracellular Vesicles*, 9, 1809064. <https://doi.org/10.1080/20013078.2020.1809064>
- Upadhy, R., Madhu, L. N., Rao, S., & Shetty, A. K. (2022). Proficiency of extracellular vesicles from hiPSC-derived neural stem cells in modulating proinflammatory human microglia: Role of pentraxin-3 and miRNA-21-5p. *Frontiers in Molecular Neuroscience*, 15, 845542. <https://doi.org/10.3389/fnmol.2022.845542>
- Warburton, E. C., & Brown, M. W. (2015). Neural circuitry for rat recognition memory. *Behavioural Brain Research*, 285, 131–139. <https://doi.org/10.1016/j.bbr.2014.09.050>
- Willis, C. M., Nicaise, A. M., Peruzzotti-Jametti, L., & Pluchino, S. (2020). The neural stem cell secretome and its role in brain repair. *Brain Research*, 1729, 146615. <https://doi.org/10.1016/j.brainres.2019.146615>
- Xie, X., Ma, G., Li, X., Zhao, J., Zhao, Z., & Zeng, J. (2023). Activation of innate immune cGAS-STING pathway contributes to Alzheimer's pathogenesis in 5xP9 mice. *Nature Aging*, 3, 202–212. <https://doi.org/10.1038/s43587-022-00337-2>
- Yang, H., Wang, H., Shu, Y., & Li, X. (2018). miR-103 promotes neurite outgrowth and suppresses cells apoptosis by targeting prostaglandin-endoperoxide synthase 2 in cellular models of Alzheimer's disease. *Frontiers in Cellular Neuroscience*, 12, 91. <https://doi.org/10.3389/fncel.2018.00091>
- Yang, H. S., Onos, K. D., Choi, K., Keezer, K. J., Skelly, D. A., Carter, G. W., & Howell, G. R. (2021). Natural genetic variation determines microglia heterogeneity in wild-derived mouse models of Alzheimer's disease. *Cell Reports*, 34, 108739. <https://doi.org/10.1016/j.celrep.2021.108739>
- Yiannopoulou, K. G., Anastasiou, A. I., Zachariou, V., & Pelidou, S. H. (2019). Reasons for failed trials of disease-modifying treatments for Alzheimer disease and their contribution in recent research. *Biomedicine*, 7, 97. <https://doi.org/10.3390/biomedicine7040097>

SUPPORTING INFORMATION

Additional supporting information can be found online in the Supporting Information section at the end of this article.

How to cite this article: Madhu, L. N., Kodali, M., Upadhy, R., Rao, S., Somayaji, Y., Attaluri, S., Shuai, B., Kirmani, M., Gupta, S., Maness, N., Rao, X., Cai, J. J., & Shetty, A. K. (2024). Extracellular vesicles from human-induced pluripotent stem cell-derived neural stem cells alleviate proinflammatory cascades within disease-associated microglia in Alzheimer's disease. *Journal of Extracellular Vesicles*, 13, e12519. <https://doi.org/10.1002/jev2.12519>